ANALYSIS OF DIFFERENT POSSIBLE DESIGNS FOR FINGERTIP SENSOR CANTILEVER BEAMS

A thesis submitted in partial fulfillment of the
requirement for the award of degree of

Master of Engineering
in
Electronic Instrumentation and Control

Submitted By
Deep Singh
800951008

Under the Guidance of
Dr. Ravinder Agarwal
Associate Professor, EIED
Head of USIC

Department of Electrical and Instrumentation Engineering
Thapar University
(Established under the section 3 of UGC act, 1956)
Patiala, 147004, Punjab, India

July11

DECLARATION

I, hereby declare that the thesis entitled "Analysis of different possible designs for fingertip sensor cantilever beams" is an authentic record of my study carried out as per the requirement for the award of degree of Masters of Engineering in Electronic Instrumentation and Control at Thapar University, Patiala.

Date:

Name-Deep Singh
Roll No: 800951008

I certify that the above statement made by the student is correct to the best of my knowledge and belief.

Date:

Dr. Ravinder Agarwal
Associate Professor, EIED
& Head of USIC
Thapar University, Patiala
Punjab

Countersigned By

S. Ghosh 22/7/11

Dr. Smarajit Ghosh
Head of department, EIED
Thapar university, Patiala
Punjab

Dr. S K Mohapatra
Dean of Academic Affairs
Thapar University, Patiala
Punjab

i

ACKNOWLEDGEMENT

"Achievement is finding out what you would be doing, what you have to do. The higher the summit, higher will be the climb." It has been rightly said that we are build on the shoulders of others but the satisfaction that accompanies the successful completion of any task would be incomplete without the mention of the people who made it possible. First, with deep sense of gratitude and hearty thanks to my project guide **Dr. Ravinder Agarwal,** EIED, Thapar University, Patiala, for their invaluable guidance to undertake the project work and being supportive at each and every step, and giving me an opportunity to understand the concept.

I am highly grateful to **Dr.Ajay Agarwal**, Scientist "E",CEERI, pilani for giving new vision to my thoughts and always ready for any type of assistance that i needed from their side. I would like to express my deep sense of gratitude towards **Dr. Smarajit Ghosh**, Professor and Head, EIED, Thapar University, Patiala who has been a constant source of inspiration for me throughout this work.

Date Deep Singh

Abstract

Prosthetic hand is an artificial device used for the functioning of a hand. There are some prosthetic hands which are controlled by using myoelectric signal (nearly 1mV) of the body. These signals are extracted with the help of electrodes which is analyzed and necessary actions like amplification, filtering is taken. These signals are further feed to microcontroller (PIC) to guide the servo motors of the hand for the control functions like wrist rotation, fingers movement, etc.

In the case of a prosthetic hand, the user is unable to 'feel' an item held by the hand. For example, the user would be unaware if he holds a very hot or very cold item, possibly resulting in damage to the prosthesis or to the user. Another example, the lack of feedback on the force exerted during a grip posture could result in the crushing of a gripped item. A possible solution to these problems is to include some form of multi-parameter sensing system within the prosthetic device. For the prosthetic hand, such a system might comprise a number of force sensors to monitor and adjust the grip strength and also include thermal sensors to measure the temperature of a grasped object. There are different static and dynamic sensors into use which are prepared by using thick-film technology. They are very suitable to measure the grip forces exerted upon an object held by a prosthetic hand. The static force sensors exploit the piezoresistive characteristics of commercially available thick-film pastes while the dynamic slip sensors utilize the piezoelectric behavior of PZT pastes.

In the present dissertation an analysis of different possible structures of cantilever beams have been carried out for the purpose of enhancing sensitivity and life of sensor. Different aspects like stress, strain, life, safety factor, deformation and hysteresis were considered for various possible shapes for the prosthetic arm.

Table of Contents

List of figures

List of tables

Chapter1

Introduction

Prosthesis is a field of medical engineering science of fusing mechanical devices with human muscle, skeleton and nervous systems to assist or enhance motor control lost by trauma, disease, or defect. Prostheses are typically used to replace parts lost by injury (traumatic) or missing from birth (congenital) or to supplement defective body parts. Various designs of artificial hands are available which are categorized as mechanical, electrical and Myo-electric hand. Mechanical devices are functional prostheses that use some motion of the body to provide the force necessary to control the prosthetic component. Electrical devices operate the hand by a motor driven by micro switches and relays. Myo-Electric hand is stimulated by muscle signal available from the stump of amputee.

Powered hand prostheses are used to replace the function of a lost natural hand. Most of the commercial prosthetic hands in clinical use are controlled by myoelectric signal and are referred to as myoelectric hands. One of the important organs of the body is the hand. We perform 90% of our daily work by hand like eating, lifting, gripping an object, writing, typing, driving etc. Many persons, especially industrial workers carrying out different type of machining tasks in the factory, lose their hands due to accidents. Their lost hand is to be replaced by an artificial hand which fulfils all the criteria of a natural hand so that the amputee may lead the life of a normal person and feels rehabilitated. In last three decades, an increasing number of handicapped persons have been provided with prosthetic hands. Surveys on using these artificial hands revealed that 30 % to 50 % of the handicapped persons do not use their prosthetic hand regularly. The main factors of the rejection of conventional prosthetic hands were heavy weight, low functionality, robot-like movement (1).

The human skin is the organ with the largest surface area on the human body. One of the main tasks of the human skin is the perception of mechanical contacts of the body's surface with the environment. This sensory system enables human to explore and manipulate the environment and to interact with it. The human hand is complex. It has 27 bones and a multitude of muscles and tendons to provide a large number of freedoms in movement. In addition, each hand has an array of over 17000 tactile sensors. Prosthesis is an artificial extension that replaces a missing

body part. Prostheses are typically used to replace parts lost by injury or missing from birth or to supplement defective body parts. In the case of a prosthetic hand, the user is unable to 'feel' an item held by the hand. For example, the user would be unaware if he holds a very hot or very cold item, possibly resulting in damage to the prosthesis or to the user. Another example, the lack of feedback on the force exerted during a grip posture could result in the crushing of a gripped item. A possible solution to these problems is to include some form of multi-parameter sensing system within the prosthetic device. For the prosthetic hand, such a system might comprise a number of force sensors to monitor and adjust the grip strength and also include thermal sensors to measure the temperature of a grasped object.

Piezoresistive and piezoelectric strain sensors are necessary tools for several industrial, automotive, aerospace and biomedical monitoring applications. There are three types of sensors used for gripping an item held by prosthetic hand which are piezoresistive thick film sensor to detect the force on finger, a piezoelectric thick film sensor to detect the onset of slip and a thick film thermistor to monitor temperature.

Finite element analysis (FEA) has been a most useful tool for analyzing stress, strain and life of different designs. Numerical solutions to even very complicated stress problems should be obtained using FEA. In spite of the great power of FEA, the disadvantages of computer solutions must be kept in mind when using this and similar methods: they do not necessarily reveal how the stresses are influenced by important problem variables such as materials properties and geometrical features, and errors in input data can produce wildly incorrect results that may be overlooked by the analyst. Perhaps the most important function of theoretical modeling is that of sharpening the designer's intuition; users of finite element codes should plan their strategy toward this end, supplementing the computer simulation with as much closed-form and experimental analysis as possible.

In this study finite element analysis of different cantilever designs have been carried out, dimensions of all these structures were set according to fingertip dimensions of natural human hand. Firstly the different slip detection techniques were studied. Thick film sensors are mostly used for the purpose of slip detection in prosthetic hand. The sensitivity and life of such sensors is greatly dependent upon the size, shape and material properties of cantilever beams. In the present dissertation an analysis of different possible structures of cantilever beams have been

carried out for the purpose of enhancing sensitivity and life of slip detection sensor in prosthetic fingers. Different aspects like stress, strain, life and deformation were considered for all the possible shapes. Influence of changing the position and contact area of los also studied. Finally, a comparative analysis of all the different structures was done along with their life and limits of force up to which these designs can work efficiently.

Chapter 2

Literature Review

Cutkosky and Tremblay (2) developed a slip sensor using accelerometers mounted on the inside of a silicone rubber skin. To allow the accelerometers to vibrate, a dome shaped piece of foam bulks out the skin producing a fingertip shape. The foam and the side of the rubber skin were both attached to a solid mounting base. The skin was made from a self-leveling silicon rubber 1.5 mm thick with small nibs on the outside surface. When slippage occur some of the nibs at the edge of the grasped object break contact and snap back to their original position causing local vibrations. These vibrations were then picked up by the accelerometers and PVDF strips which were attached to the underside of the skin. The signals obtained from the accelerometer had been successfully used in conjunction with a tangential normal force sensor to control a five linkage robotic finger, limiting the slip of an object occurring even when a sudden change in load was applied.

Mingrino (3) investigated a method to detect the incipient slip by monitoring the normal and shear force from a grasped object. The force sensor used comprised four piezoresistive thick-film force sensors printed on a polymer film in a square configuration with each sensor being printed in a triangular shape pointing towards the center of the square. The force applied by gripping an object was coupled to the center of the sensor configuration via a cylinder. The normal force and tangential force of the object was calculated from the force ratios applied to each thick-film resistor. By monitoring the normal and tangential forces and keeping the normal to tangential force ratio above a predefined level sets the lowest coefficient of friction limit to that value. Below this value, determined by the properties of the prosthesis glove and object, slip will occur and conversely above that value no slip will occur. It was, therefore, advantageous to set a high safety factor, allowing a range of objects to be gripped.

MARCUS project (4) was a prosthetic hand controlled by the user through myoelectric sensors. The hand was equipped with position, force and slippage sensors through which a microprocessor automatically controls the interaction of the hand with the object. The control strategy allows to automatically increment the force on the grasped object if slippage conditions

occur. Two separate categories of exteroceptive sensors had been discovered i:e static and dynamic sensors, while only one category for proprioception i:e kina esthetic sensors.

Dario *et al*. (5) developed a fingertip sensor for uses on a robotic arm and used an overlapping configuration of eight rows and eight columns of piezoresistive silk-screened ink, to create an array of 64 force sensors. A piezoelectric ceramic bimorph element was also attached to the fingertip to be used as a dynamic force sensor in an attempt to detect slip. The piezoresistors had a measuring force range of 0.1–8 N with a maximum spatial resolution of 1 mm, which is the maximum resolution that a human fingertip can differentiate between two different objects.

Artificial hand that meets the requirements of a improved prosthetic hand was developed at the Forschungszentrum Karlsruhe (6). It was based on the so called flexible fluidic actuators. The miniaturized actuators were integrated in the fingers of the new artificial hand. Total of 18 miniaturized flexible fluidic actuators were integrated into the mechanical construction of the fingers and the wrist of the hand. Fingers contain the flexible fluidic actuators that lead to a flexion of the finger, flex sensors and touch sensors. Metacarpus provides enough space to house a microcontroller, micro valves, the energy source and a micro pump. Wrist (optional): also contains flexible fluidic actuators that bend the wrist.

The hand was designed to augment the dexterity of traditional prosthetic hands while maintaining the same dimension and weight. The approach was aimed at providing enhanced grasping capabilities and natural sensory-motor coordination to the amputee, by integrating miniature mechanisms, sensors, actuators, and embedded control. A Biomechatronic hand prototype with three fingers and a total of six independent DOFs had been designed and fabricated. The Otto Bock hand has only one degree of freedom (DOF) it can move the fingers at proportional speed from 15–130 mm/s and can generate a grip force up to 100 N (7).

To detect the slip movements in prosthetic hands capacitance effects were used, which were measure the strain on elastic polymer foam. Low power consumption results in device that can be supplied from a miniature battery thereby requiring only Signal wires to the controller. A non-linear model accurately describes the Characteristic of the sensor, requiring the estimation of only three parameters. The sensor was consists of two parallel plates separated by an elastic

material that also acts as a dielectric. Applying a force across the plates increases the capacitance and accordingly the slip was detected (8).

Thick-film static and dynamic force sensors had been investigated for their suitability to measure the grip forces exerted upon an object held by a prosthetic hand, and to detect and correspondingly react to the possible slip of a gripped item (9). The static force sensors exploit the piezoresistive characteristics of commercially available thick-film pastes whilst the dynamic slip sensors utilize the piezoelectric behavior of PZT (lead zirconate titanate) pastes. The sensors were located upon stainless steel cantilever type structures that will be placed at the fingertips of each digit of the prosthetic hand. Temperature sensors were also included to provide temperature compensation for the force sensors and to prevent accidental thermal damage to the prosthesis.

The design and development of a silicon-based three-axial force sensor to be used in a flexible smart interface for biomechanical measurements was discussed. Normal and shear forces were detected by combining responses from four piezoresistors obtained by ion implantation in a high aspect-ratio cross-shape flexible element equipped with a 525 µm high silicon mesa. Piezoresistor size ranges between 6 and 10 µm in width, and between 30 and 50 µm in length. The sensor configuration follows a hybrid integration approach for interconnection and for future electronic circuitry system integration (10).

An array of sensors on a fingertip shaped beam was produced using thick-film printing techniques. There were three types of sensors used for gripping an item held by prosthetic hand which are piezoresistive thick film sensor to detect the force on finger, a piezoelectric thick film sensor to detect the onset of slip and a thick film thermistor to monitor temperature. The temperature sensor was used to detect if an object gripped by the hand is too hot or too cold, and thus prevent damage to the prosthesis by automatically releasing the object (11).

The embedded hardware architecture, had been designed in order to allow exchanging information with the subject either employing a non-invasive UPI (Classical EMG control, plus tactile display), in the short term, or an invasive neural interface connected to the peripheral nervous system, in the long term. The design of flexible embedded control architecture for the action and perception of an anthropomorphic with 16 degree of freedom, 4 degree of actuation had been discussed for use of prosthetic hand amputees. The prosthetic hand was provided with

40 structurally integrated sensors useful both for automatic grasp control and for biofeedback delivery to the user through an appropriate interface (12).

This sensor was recognized for detecting different phases of contact including stretching work or object grasping. Only one micro sensor was employed for this design reducing the difficulties in making soft finger tips. This sensor was constructed by using micro electro mechanical system technology, which was able to detect three forces and moments. Principles of operation of the sensor were described, along with a circuit model for calibration and data acquisition. Experiments were designed to investigate the responses of the sensor when these finger tips were used in applications related to tactile perception (13).

Tactile slip sensor for an anthropomorphic robot hand was discovered, the measurement circuit and the corresponding algorithm to determine slip states were discussed (14). The main slip sensor components consist of a silicone rubber surface which covers a PVDF sensor. The amplification of the signal was done and then the amplified signal was processed through discrete short-time fourier transform. The PVDF were highly sensitive to mechanical deformation and generates electrical charge when it was deformed. These electrodes were covered with conductive foam and the application of a pressure on this sensor leads to a drop of resistance to be measured between the sensing electrodes and the common electrodes.

To investigate more sophisticated prosthetic hand, several methods of object slip prevention were implemented with the Motion Control Hand (Motion Control, Inc. Salt Lake City, UT.). Proportional and proportional derivative shear force feedback slip prevention controllers were developed as well as an adaptive slip prevention system. When slip was detected, the adaptive controller subsequently increases and maintains a larger grip force to prevent future occurrences of slip, as in human grasping operations. Motion Control Hand was equipped with six strain gages mounted on the thumb which were used to measure the normal and shear forces. The arrangements of the strain gauges enable the measurement of forces in two directions. The Motion Control Hand had one degree of freedom (15).

Today's commercial prosthetic hands were not giving any conscious sensory feedback to overcome this deficiency in prosthetic hands, new methods were investigated, which proposed a sensory feedback system utilized tactile display on the remaining amputation residual limb acting

as man-machine interface (16). A sensory feedback system consisting of five actuators, control electronics and a test application running on a computer had been designed and built. Each finger was represented by actuator providing spatial and force sensory feedback on the forearm.

This sensor exploits the unusual resistance change that occurs when the pressure conductive rubber undergoes shear deformation (17). In the slip sensor, two electrodes were alternately coiled around a spiral structure, and pressure conductive rubber (6 mm×6 mm) rests on the electrodes. The electrode was connected to a DC power supply (5 V) through a resistance of 1 kΩ. The voltage potential between the electrodes from the Vc terminal was converted into a digital signal, and signal processing was performed on a PC.

A one-dimensional theory was developed for modeling the analysis of beams containing piezoelectric sensors and actuators. The equations of motion and associated boundary conditions were derived for the vibrations of piezoelectrically actuated beams. The effect of coupling between longitudinal deflection and bending deflection was investigated. The proposed beam theory as well as the finite element approach was used in developing a formal two-dimensional theory for piezoelectrically actuated composite plates and shells or other physical systems (18).

Bimorph-type bending actuators had been widely used in many applications as converters of electric input to mechanical motion, or vice versa. A new piezoelectric model of a multilayer piezoelectric cantilever was obtained, and the analytic expressions for the curvature, displacement and tip-deflection of the multilayer structure were derived in the static state. With the use of this model and the solution, the tip deflections of the piezoelectric bimorph cantilever in different working situations were compared and the effect of the metal electrodes on the tip-deflection of the cantilever was considered (19).

A predictive model for the deflection and profile of poly-SiGe beams for different thicknesses and geometries were evaluated. The structure employed to derivate the stress gradient and to calibrate and test the FEA calculations was a cantilever beam with dimensions of 1mm length, 100 micrometer breadth, 10 micrometer thickness. The stress gradient of film was obtained by measuring the deflection of the cantilevers with different etch depths. The deflection of the beam was calculated initially using a 2D plane stress model. The influence of the clamping region on the deflection was studied by using a perfect clamped beam and compared with a beam clamped

only at the bottom clamp interface. FEM had been successfully applied to calculate the deflection of SiGe cantilever beams (20).

Bio-Micro Electro Mechanical Systems/Nano Electro Mechanical Systems include a wide variety of sensors, actuators and complex micro/nano devices for biomedical applications. A simple cantilever beam was used as a sensor for biomedical, chemical and environmental applications, where micro fabricated multilayered cantilever beam was exposed to sensing environment. Lower layer being pure structural silicon or polymer and upper layer was of polymer with antigen/antibody immobilized in it. In the model analysis, both weight and surface stress effects on the cantilever were considered (21).

Coated cantilever beams were complex and many authors had offered solutions using analytical techniques. The FEMLAB finite-element multiphysics package was used to incorporate the full magnetostrictive strain tensor and couple it with partial differential equations from structural mechanics to solve simple cantilever systems. A wide range of geometries and material properties were solved to study the effects on cantilever deflection and the system resonance frequencies. The models were tailored for comparison with other such data within the field and results also go beyond previous work (22).

The deformation of a soft fingertip was investigated when a object through it starts sliding. This process was simulated using ANSYS software with non-linear Finite Element Analysis (FEA). Based on the results of this simulation, the experiments were designed to observe the sliding and object grasping of a soft fingertip, in which, a 4-DOF (degree of freedom) micro force/moment sensor was embedded inside the soft fingertip. With this sensor, values of force and moment acting in the fingertip were measured, based on the piezoresistive effect. These measurements provide information on the status of contact and sliding of a soft fingertip on a surface (23).

Silicon cantilevers were used as principal sensing components in measuring physical parameters, chemical and biochemical sensing, and monitoring DNA changes. Finite element method was employed for design implementation. Design target is to achieve high sensitivity in bending without the use of fluorescence or radioactive label. Design parameters under consideration were length and thickness of the cantilever. Finite element model was developed as a thin cantilever of uniform rectangular cross-section discredited with 8-node quadrilateral brick element. Linear

static stress analyses were performed to extract the amount of bending and the stress induced by different loadings. Finite element modeling and design analysis were implemented in general-purpose FE code (24).

Objective

Piezoresistive and piezoelectric thick film sensors are the latest and most widely used force and slip detecting systems for prosthetic hand. Sensitivity and life of sensor is greatly depended upon shape and size of cantilever structure. In the present dissertation work emphasize was given to different possible designs of cantilevers for slip detecting sensor in prosthetic fingertips to enhance sensitivity and life, while reducing size and weight. Finite element analysis of different possible designs of cantilever beams have been carried out using ANSYS simulation tool, for the purpose of investigating more and more efficient structures in different regards like sensitivity, life and ability to handle different(heavy/light) loads.

Chapter 3

Methodologies For Slip Detection

3.1 Introduction

In the case of a prosthetic hand, the user is unable to 'feel' an item held by the hand. For example, the user would be unaware if he holds a very hot or very cold item, possibly resulting in damage to the prosthesis or to the user. Another example, the lack of feedback on the force exerted during a grip posture could result in the crushing of a gripped item. A possible solution to these problems is to include some form of multi-parameter sensing system within the prosthetic device. Piezoresistive and piezoelectric strain sensors are necessary tools for several industrial, automotive, aerospace and biomedical monitoring applications. There are three types of sensors used for gripping an item held by prosthetic hand: Piezoresistive thick film sensor to detect the force on finger, a piezoelectric thick film sensor to detect the onset of slip and a thick film thermistor to monitor temperature. With the advancement of technology more and more efficient ways of slip detection in prosthetic hands have been investigated, much attention has been given to enhance sensitivity and life of sensor.

3.2 Different approaches for slip detection in prosthetic hand

3.2.1 Capacitance type sensors

The sensor consists simply of two parallel plates separated by an elastic material that also acts as a dielectric. Applying a force across the plates increases the capacitance. The material between the two plates should yield sufficiently under low loads, in an ideal elastic (no hysteresis) and repeatable manner. The obvious material is spring steel since this has the potential to produce a sensor with little hysteresis. A material that fills the whole space between the two plates would make construction of the device both easier and therefore less expensive to manufacture. Polymer foams with suitable mechanical and electrical properties were used. These were bonded between two brass shims (300 mm^2) with cyanoacrylate. The whole assembly was bonded to a very high density polycarbonate strip to provide a stable platform. Different components of the sensor are shown in Figure 3.1.

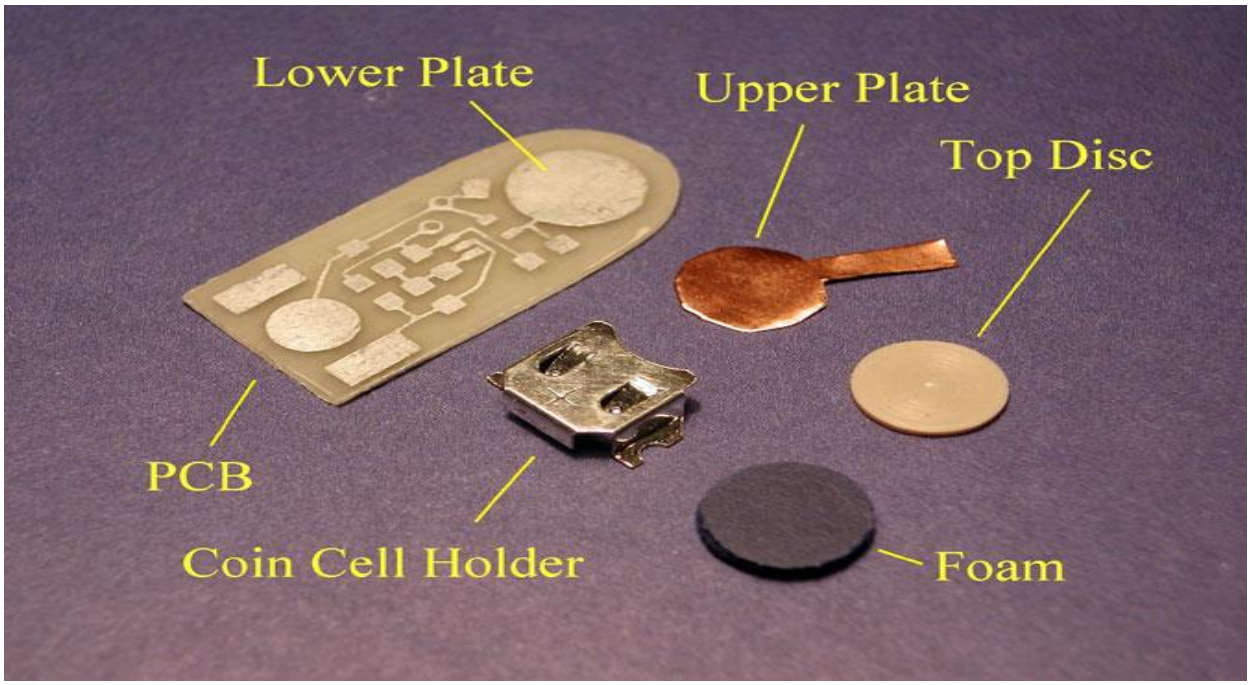

Figure 3.1 Capacitive fingertip sensor

3.2.2 Pressure conductive rubber slip sensor

It is a thin (0.5 mm) and flexible slip sensor composed of pressure conductive rubber. This sensor exploits the unusual resistance change that occurs when the pressure conductive rubber undergoes shear deformation. In the slip sensor, two electrodes are alternately coiled around a spiral structure, and pressure conductive rubber (6 mm×6 mm) rests on the electrodes. The electrode is connected to a DC power supply (5 V) through a resistance of 1 kΩ. The voltage potential between the electrodes from the Vc terminal is converted into a digital signal, and signal processing is performed on a PC. Therefore, the sensor output is digital output that indicates whether or not the object slips. Since this sensor uses rubber, it is light-weight and low-profile (2.0 mm). Figure 3.2 shows the structure of the sensor.

3.2.3 PVDF type slip sensor

The main slip sensor components consist of a silicone rubber surface which covers a PVDF (polyvinylidene fluoride) sensor. After the amplification of the signal it is processed by a discrete short-time fourier transform. Sensor assembly is shown in Figure 3.3. The PVDF is highly sensitive to mechanical deformation and generates electrical charge when it is deformed. Main components of this sensor type are a common electrode and sensing electrodes which are

arranged as a matrix. These electrodes are covered with conductive foam and the application of a pressure on this sensor leads to a drop of resistance to be measured between the sensing electrodes and the common electrode. The PVDF provides a charge depending on the mechanical deformation of polymer film. This charge changes over time t when mechanical deformation changes over time. Instrument amplifier has been used to amplify the charge signal.

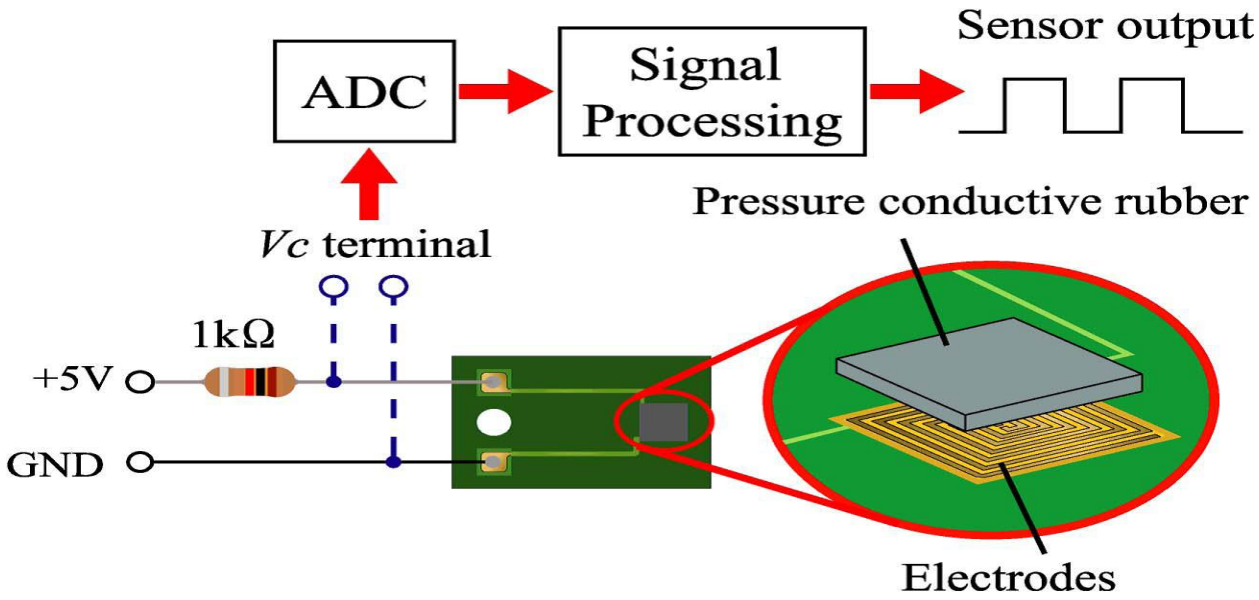

Figure 3.2 Sensor structure

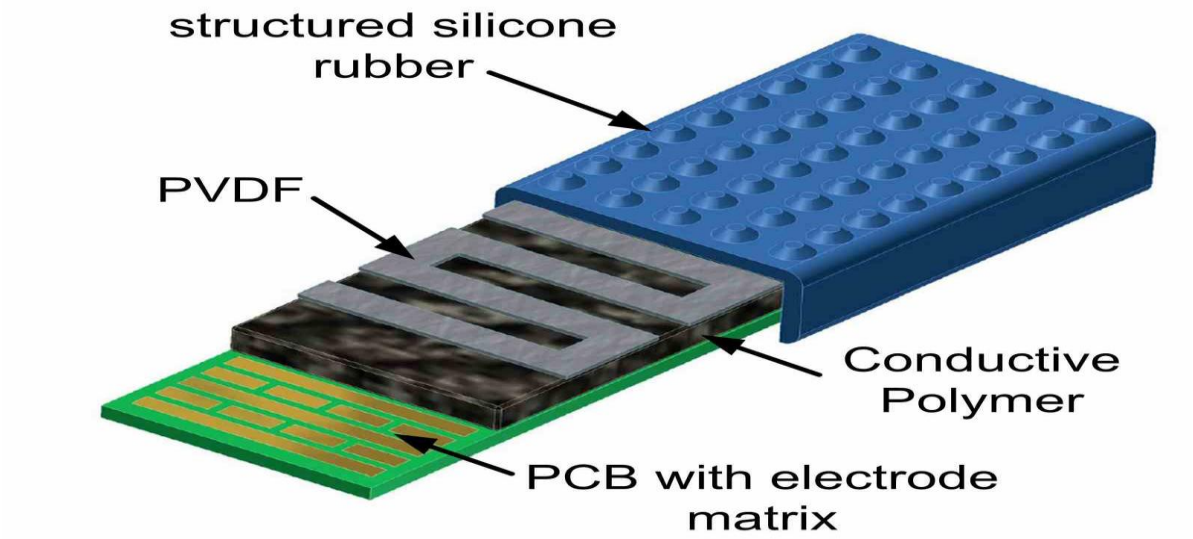

Figure3.3 Sensor assembly

3.2.4 Silicon micro sensor

This sensor can be applied in medical applications where the keyword requirements are three-axial force measurement and miniaturization. The device has been designed in order to develop a flexible smart interface to be used to detect the forces to which the stump skin tissue is subjected while in contact with the socket worn by above knee amputees. In addition, the mechanical characteristics of the sensor have also been assessed as appropriate for the sensory system of artificial hands. Four piezoresistors are used independently in order to measure the three components of applied forces through a resistance change, and the sensor cross-shape guarantees the mechanical decoupling of the shear components of the applied load. The implemented hybrid silicon micro system allows the assembling of an array of devices in a flexible substrate. The flexible array is embedded in skin like materials that act as a mechanical interface between the sensor array and the external world. The maximum pressure applied locally at the socket has been estimated as P = 0.329 MPa that corresponds to a normal load Fnormal = 0.26 N when considering a contact circular area of 1mm diameter. With an average friction coefficient between stump and socket $\mu = 0.8$, the maximum shear stress that is applied locally is $\tau = \mu P$ = 0.26 MPa corresponding to a shear load Fshear = 0.21 N.

3.2.5 Thick film slip sensors

Thick-film static and dynamic force sensors have been used effectively for their suitability to measure the grip forces exerted upon an object held by a prosthetic hand, and to detect and correspondingly react to the possible slip of a gripped item. The static force sensors exploit the piezoresistive characteristics of commercially available thick-film pastes whilst the dynamic slip sensors utilize the piezoelectric behavior of PZT (lead zirconate titanate) pastes. The sensors are located upon stainless steel cantilever type structures that will be placed at the fingertips of each digit of the prosthetic hand. Temperature sensors are also included to provide temperature compensation for the force sensors and to prevent accidental thermal damage to the prosthesis. Results have shown that the static force sensor is capable of measuring fingertip forces in excess of 100 N, with an electrical half-bridge configuration sensitivity approaching 10 $\mu V (VN)^{-}$ (with scope for improvement) and maximum hysteresis below 4% of full scale, depending on the manner in which the cantilever sensor array is attached to the fingers. The cantilever is machined

from grade 304 stainless steel and has a nominal thickness of 3 mm, which may be changed (along with the beam width) to adjust the sensitivity and/or the measurement range of the device.

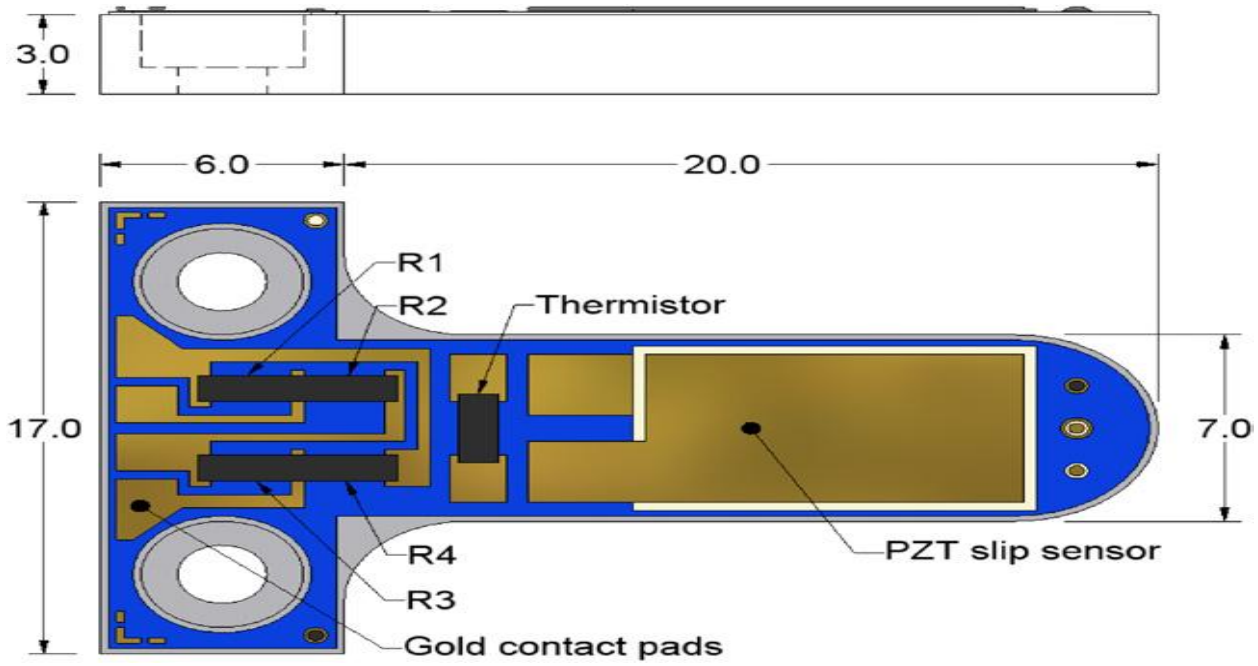

Figure 3.4 Thick film slip sensor

3.2.6 Centre of pressure slip detection

Centre of pressure sensors can measure the center position of a distributed load applied to the surface of the sensor and the total load itself within 1 ms. Thus, rapid slip detection can be achieved. Centre of pressure sensors can measure the center position of a distributed load and the total load itself. The structure of the centre of pressure sensor consists of pressure sensitive material (pressure conductive rubber) sandwiched between two sheets of conductive film, Layers A and B (upper and lower layers respectively). Both edges of the conductive film are electrodes, and we can derive the center position of the current distribution from the potential difference of the electrodes on both conductive film layers.

3.2.7 Micro force/moment sensor

This sensor can recognize many phases of contact in grasping including stretching work or object grasping. Only one micro sensor was employed for this design reducing the difficulties in making soft finger tips. This sensor was constructed by using micro electro mechanical system

technology, which is able to detect three forces and moments. The MFMS chip, which can detect independently three components of force (Fx, Fy, Fz) and three components of moment (Mx, My, Mz) is connected to a soft contact part (a silicone rubber hemisphere) by a silicon transmission pillar. The overload protection base, made of pyrex, is located under the chip to protect MFMS chip from overloading. Gold wire bonding was used to connect the chip and the printed circuit board (PCB), and both the chip and the protection base are covered by ceramic case. The overall dimensions of sensor are 11 mm, 5 mm, 3.3 mm. Different components of the micro force moment sensor have been shown in Figure 3.6.

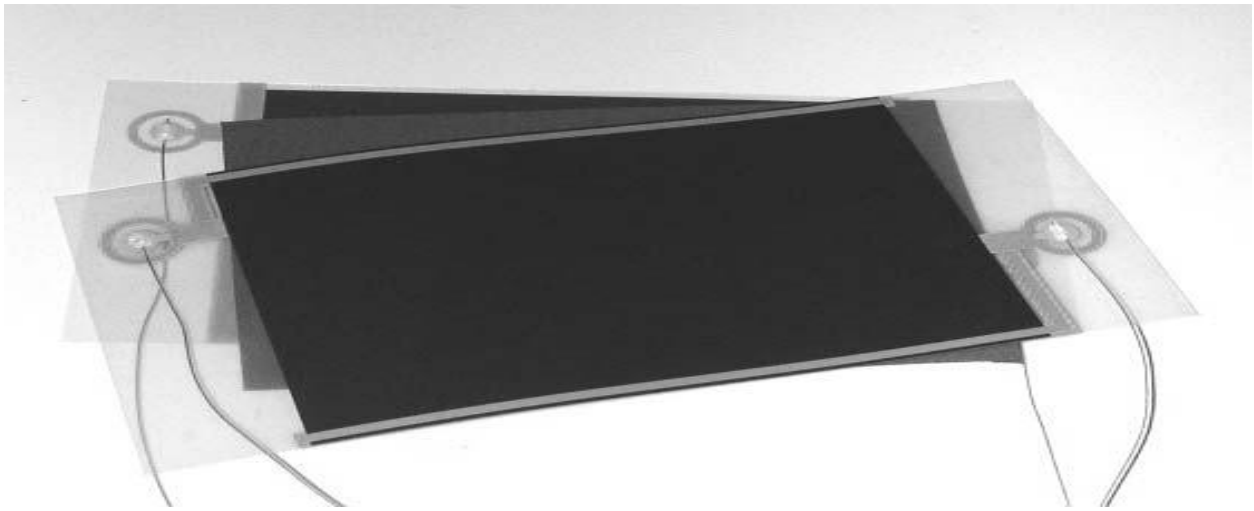

Figure 3.5 CoP sensor

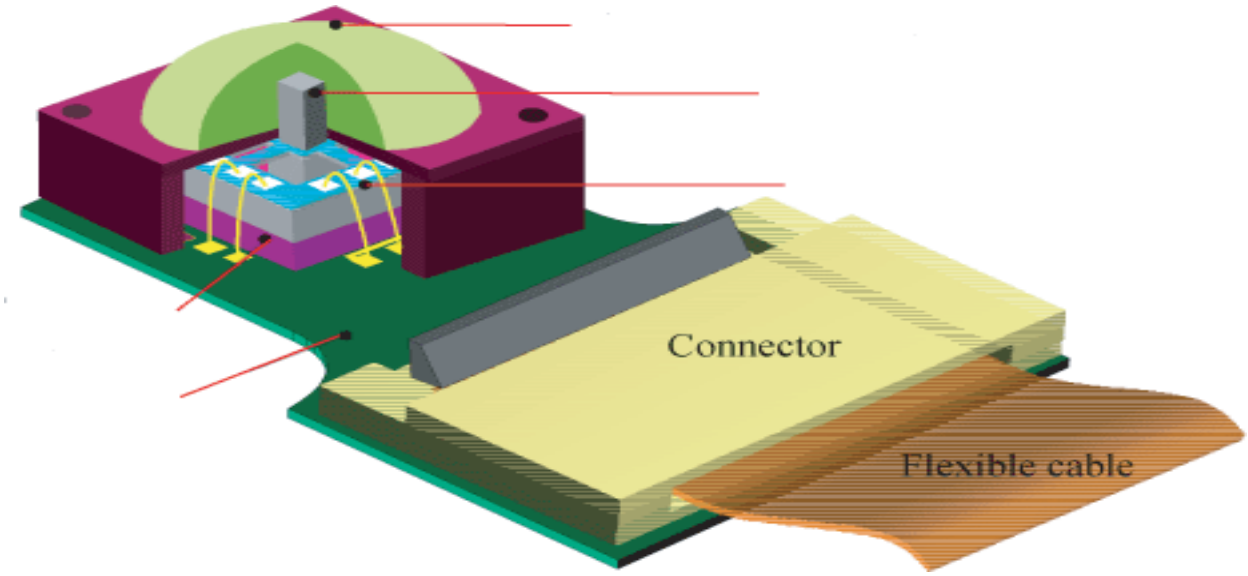

Figure3.6 MFMS system

3.3 limitations of current slip detection techniques

- The main drawbacks associated with the capacitive approach are the inherently nonlinear output of the sensor and the complexity of electronics.
- In the pressure conductive rubber sensor it is difficult to separate the resistance change caused by the normal force and the resistance change caused by object slip, so we have to follow a large processing.
- There are number of limitations with PVDF type of sensor such as a low sensitivity of around 20–30 pC/N and a high sensitivity to temperature change. The sensor activity changes by approximately 0.5 % per C, which in the operating temperature range of a prosthetic hand of -30° C in cold conditions to 50° C (or potentially higher) when holding a hot object means a 40 % change in the activity of the sensor would occur.
- Silicon micro sensors are best suitable for above knee amputees, they have very low sensitivity for low pressure input.
- MFMS chips have large dimensions and complex fabrication procedure also they are not sensitive enough for low speed slip detections.
- Centre of pressure sensor is the latest technique having some good features but does not find much application in the commercial uses.

3.4 Requirements

The requirements for a good slip detecting sensor are that it should have the following characteristics.

- Resolve forces up to 100 N
- Not susceptible to EM interference
- High sensitivity to small forces
- Not easily damaged by large impact forces
- Integral power supply Robust
- Lightweight Service period of six months
- Low cost
- Simplicity in construction and mounting

- Little hysteresis
- Small size with an area less than 100 mm^2
- Low power consumption
- Thin in depth for mounting on fingers and palm

Chapter4

ANSYS Workbench

4.1 Introduction

ANSYS is a general purpose finite element modeling package for numerically solving a wide variety of mechanical problems like static and dynamic structural analysis for both linear and non-linear, heat transfer and fluid problems, as well as acoustic and electro-magnetic problems. A fundamental premise of using the finite element procedure is that the body is sub-divided into small discrete regions known as finite elements. These elements are defined by nodes and interpolation functions. Governing equations are written for each element and these elements are assembled into a global matrix. Loads and constraints are applied and the solution is then determined. It uses a preprocessor software engine to create geometry. Then it uses a solution routine to apply loads to the meshed geometry. Finally it outputs desired results in post-processing. Finite element analysis was first developed by the airplane industry to predict the behavior of metals when formed for wings. The objective of this chapter is to briefly introduce ANSYS workbench and the different steps through which a user has to go that is preprocessing, solution routine and post processing steps. Application of solid model loading, mesh generation and fatigue analysis tools in ANSYS workbench are discussed.

4.2 Different steps to work with ANSYS

A finite element solution may be broken into the following three stages. This is a general guideline that can be used for setting up any finite element analysis. The Main menu is designed so that you should complete the steps required to build your model by beginning at the top of the menu and working your way down.

1. Preprocessing: defining the problem; the major steps in preprocessing are given below:

- Define key points/lines/areas/volumes
- Define element type and material/geometric properties
- Mesh lines/areas/volumes as required

- The amount of detail required will depend on the dimensionality of the analysis (i.e. 1D, 2D, axisymmetric, 3D).

2. Solution: assigning loads, constraints and solving; here we specify the loads (point or pressure), constraints (translational and rotational) and finally solve the resulting set of equations. Most loads are applied either on the solid model (on key points, lines, and areas) or on the finite element model (on nodes and elements). Different types of loads available in ANSYS workbench are presented below.

- Structural: displacements, forces, pressures, temperatures (for thermal strain), gravity
- Thermal: temperatures, heat flow rates, convections, internal heat generation, infinite surface.
- Magnetic: magnetic potentials, magnetic flux, magnetic current segments, source current density, infinite surface.
- Electric: electric potentials (voltage), electric current, electric charges, charge densities, infinite surface.
- Fluid: velocities, pressures.

3. Post processing: further processing and viewing of the results; in this stage one may wish to see:

- Lists of nodal displacements
- Element forces and moments
- Deflection plots
- Stress contour diagrams

4.3 Solid modeling within ANSYS

In ANSYS terminology model generation usually takes on the narrower meaning of generating the nodes and elements that represent the spatial volume and connectivity of actual system. Thus model generation in this discussion means the process of defining geometric configurations of the model's nodes and elements. Typical steps involved for model generation in ANSYS are outlined below:

- Begin by planning your approach. Determine objectives, decide what basic form your model will take, choose appropriate element types and consider how you will establish an appropriate mesh density. You will typically do this general planning before you initiate the ANSYS workbench
- Enter the preprocessor to initiate your model building session. Most often you will build your model with solid modeling procedures
- Establish working plane
- Generate basic geometric feature using geometric primitive and Boolean operator.
- Activate the appropriate coordinate system
- Generate other solid model features from bottom up. That is, create key points, and then define lines, areas and volumes as needed
- Use more Boolean operators or number controls to join separate solid model regions together as appropriate
- Create tables of element attributes (element types, real constants, material properties and element coordinate system)
- Set element attribute pointer
- Set meshing controls to establish your desired mesh density if desired
- Create nodes and elements by meshing your solid model
- After you have generated nodes and elements add features such as surface to surface contact elements, coupled degrees of freedom and constraint equations
- Save your model
- Exit the preprocessor

4.4 Mesh generation

From easy automatic meshing to a highly crafted mesh, ANSYS provides the ultimate solution. Powerful automation capabilities ease the initial meshing of a new geometry by keying off physics preferences and using smart defaults so that a mesh can be obtained upon first try. Additionally, users are able to update immediately to a parameter change, making the handoff from CAD to CAE seamless and aiding in up-front design. Once the best design is found, meshing technologies from ANSYS provide the flexibility to produce meshes that range in

complexity from pure hex meshes to highly detailed hybrid meshes; users can put the right mesh in the right place and ensure that a simulation will accurately validate the physical model. ANSYS has a range of meshing tools that cater to nearly all physics. While the meshing technologies were developed to meet specific needs in the areas of solid, fluid, electromagnetic shell, 2-D and beam models, access to these technologies is available across all physics.

For solid models meshing technologies from ANSYS provide robust, well-shaped quadratic tetrahedral meshing on even the most complicated geometries. With automatic contact detection and setup, a user requires little training to perform sophisticated analysis. In addition, users can generate pure hex meshes using one of several mesh methods, depending on the type of model and whether the user wants a pure hex mesh or a hex-dominant mesh. ANSYS meshing technologies provide physics preferences that help automate the meshing process. For an initial design, a mesh can often be generated in batch with an initial solution run to locate regions of interest. Further refinement can then be made to the mesh to improve the accuracy of the solution. There are physics preferences for structural, fluid, explicit and electromagnetic simulations. By setting physics preferences the software adapts to more logical defaults in the meshing process for better solution accuracy.

Shell modeling and meshing solutions from ANSYS offer numerous approaches that provide meshes that best meet the physics. In general, this consists of two approaches that use common tools:

- 2-D axisymmetric or planar models can be used to simplify 3-D physics in a 2-D fashion. 2-D models can be meshed with quad meshes, quad-dominant meshes or all-triangle meshes.
- Shell models can be used to simplify 3-D models to a set of sheets with a defined thickness. This is particularly useful for modeling sheet metal or thin structural parts. Shell parts can also be meshed with quad meshes, quad-dominant meshes or all-triangle meshes.

4.5 Solid-model loading

Loads in ANSYS workbench are applicable on nodes, key points, element faces and special

regions generated using design modeler. A load step is simply a configuration of loads for which a solution is obtained. In a linear static or steady-state analysis, you can use different load steps to apply different sets of loads -wind load in the first load step, gravity load in the second load step, both loads and a different support condition in the third load step, and so on. In a transient analysis, multiple load steps apply different segments of the load history curve. Loads are divided into six categories:

- DOF constraints
- Forces (concentrated loads)
- Surface loads
- Body loads
- Inertia loads
- Coupled-field loads

A DOF constraint fixes a degree of freedom (DOF) to a known value. Examples of constraints are specified displacements and symmetry boundary conditions in a structural analysis, prescribed temperatures in a thermal analysis, and flux-parallel boundary conditions. A force is a concentrated load applied at a node in the model. Examples are forces and moments in a structural analysis, heat flow rates in a thermal analysis, and current segments in a magnetic field analysis. A surface load is a distributed load applied over a surface. Examples are pressures in a structural analysis and convections and heat fluxes in a thermal analysis. Solid-model loads are independent of the finite element mesh. That is you can change the element mesh without affecting the applied loads. This allows you to make mesh modifications and conduct mesh sensitivity studies without having to reapply loads each time. The solid model usually involves fewer entities than the finite element model. Therefore, selecting solid model entities and applying loads on them is much easier, especially with graphical picking.

4.6 ANSYS solvers

Several methods of solving the system of simultaneous equations are available in the ANSYS program:

- Sparse direct solution

- Frontal direct solution
- Jacobi Conjugate Gradient (JCG) solution
- Incomplete Cholesky Conjugate Gradient (ICCG) solution
- Preconditioned Conjugate Gradient (PCG) solution
- Automatic iterative solver option (ITER)

The sparse direct solver is the default solver for all analyses, except for electromagnetic analyses, analyses that include both p-elements and constraint equations, spectrum analyses, and sub structuring analyses (which each use the frontal direct solver by default).

4.7 Methodology for Structural stress, strain and deformation evaluation

In the ANSYS workbench there is different methodology available for the calculation of different parameters. The different ways of stress strain calculation regions like integration point, surface and combined strain and stress are developed. Although in this study we are only limited to Von Mises surface stress and strain equations, but the needed basic equations are also derived.

4.7.1 Integration point strains and stresses

Stress is related to strain by the equation :

$$\{\sigma\} = [D]\{\varepsilon^{el}\} \quad (1)$$

Where

$\{\sigma\}$ = stress vector

$[D]$ = elastic stiffness matrix

$\{\varepsilon^{el}\} = \{\varepsilon\} - \{\varepsilon^{th}\}$ = elastic strain vector

$\{\varepsilon\}$ = total strain vector

$\{\varepsilon^{th}\}$ = thermal strain vector

The principal of virtual work states that virtual (very small) change of the internal strain energy must be offset by an identical change in external work due to the applied loads.

$$\delta U = \delta V \quad (2)$$

Where

U = strain energy (internal)

V= virtual work

δ = virtual operator

Now the element integration point strains and stresses are computed by combining equations (1) and (2) to get equations (3) and (4) respectively.

$$\{\varepsilon^{el}\} = [B]\{u\} - \{\varepsilon^{th}\} \quad (3)$$

$$\{\sigma\} = [D]\{\varepsilon^{el}\} \quad (4)$$

Where

$\{\varepsilon^{el}\}$ = strain that causes stresses

[B]= strain-displacement matrix evaluated at integration point

{u} = nodal displacement vector

$\{\varepsilon^{th}\}$ = thermal strain vector

{σ} = stress vector

[D] = elasticity matrix

4.7.2 Surface stresses

Surface stress output may be requested on free faces of 2-D or 3-D elements. Free means not connected to other elements as well as not having any imposed displacements or nodal forces normal to the surface. The following steps are executed at each surface gauss point to evaluate surface stresses.

1. Compute the in plane strains of the surface at an integration point using :

$$\{\epsilon'\} = [B']\{u'\} - \{(\varepsilon^{th'})\} \quad (5)$$

Hence $\varepsilon'_x, \varepsilon'_y$ and ε'_z are known. The prime (‘) represents the surface coordinate system, with z being normal to the surface.

(2) At each point set :

$$\sigma'_z = -\mathrm{P} \quad (6)$$

$$\sigma'_{xz} = 0 \quad (7)$$

$$\sigma'_{yz} = 0 \quad (8)$$

Where P is the applied pressure

(3) At each point use the six material property equation represented by :

$$\{\sigma'\} = [\mathrm{D'}]\{\varepsilon'\} \quad (9)$$

To compute the remaining strain and stress components (ε'_z , ε'_{xz} , ε'_{yz} , σ'_x , σ'_y and σ'_{xy}).

(4) Repeat and average the results across all integration points.

4.7.3 Combined strains and stresses

When a model has only one functional direction of stress and strains, comparison with allowable value is straight forward. But when there is more than one component, the components are combined normally into one number to allow a comparison with an allowable.

The principal strains are calculated from the strain components by the cubic equation :

$$\begin{vmatrix} \varepsilon_x - \varepsilon_0 & -\frac{1}{2}\varepsilon_{xy} & \frac{1}{2}\varepsilon_{xz} \\ \frac{1}{2}\varepsilon_{xy} & \varepsilon_y - \varepsilon_0 & \frac{1}{2}\varepsilon_{yz} \\ \frac{1}{2}\varepsilon_{xz} & \frac{1}{2}\varepsilon_{yz} & \varepsilon_z - \varepsilon_0 \end{vmatrix} = 0$$

where ε_0 =Principle strains

The Von Mises or equivalent strains ε_e is computed as

$$\varepsilon_e = \frac{1}{1+v'}\left(\frac{1}{2}\left[(\varepsilon_1-\varepsilon_2)^2+(\varepsilon_2-\varepsilon_3)^2+(\varepsilon_3-\varepsilon_1)^2\right]\right)^{\frac{1}{2}} \quad (10)$$

v' =effective Poisson's ratio

The principal stresses are calculated from the stress components by the cubic equation :

$$\begin{vmatrix} \sigma_x - \sigma_0 & \sigma_{xy} & \sigma_{xz} \\ \sigma_{xy} & \sigma_y - \sigma_0 & \sigma_{yz} \\ \sigma_{xz} & \sigma_{yz} & \sigma_z - \sigma_0 \end{vmatrix} = 0$$

Where σ_0 is principal stress

The Von Mises or equivalent stress are computed by equation :

$$\sigma_e = \left(\frac{1}{2}\left[(\sigma_1-\sigma_2)^2+(\sigma_2-\sigma_3)^2+(\sigma_3-\sigma_1)^2\right]\right)^{\frac{1}{2}} \quad (11)$$

4.7.4 Deformation

The applied loads acting on a body make it move from one position to other. The structure under load gets deformed due to change in position of atoms. This motion can be defined by studying the position vector in the deformed and un-deformed configurations. If the position vectors in deformed and un-deformed states are represented by {X} and {x} then the displacement vector {u} is computed by equation :

$$\{u\}=\{x\} - \{X\} \quad (12)$$

The deformation gradient is defined as

$$[F] = \frac{d\{x\}}{d\{X\}} \quad (13)$$

Which can be written as in the terms of displacement of the point via equation (12) as :

$$[F] = [I] + \frac{d\{u\}}{d\{X\}} \quad (14)$$

Where [I]= identity matrix, the information contained in the deformation gradient [F] the volume change, the rotation and shape change of the deforming body. The volume change at a point is given by equation:

$$\frac{d\{V\}}{d\{V_0\}} = \det[F] \quad (15)$$

Where

V_0= original volume

V= current volume

4.8 Fatigue analysis tools

The focus of fatigue in ANSYS is to provide useful information to the design engineer when fatigue failure may be a concern. Fatigue results can have a convergence attached. A stress-life approach has been adopted for conducting a fatigue analysis. Several options such as accounting for mean stress and loading conditions are available. A large part of a fatigue analysis is getting an accurate description of the fatigue material properties. Since fatigue is so empirical, sample fatigue curves are included only for structural steel and aluminum materials. These properties are included as a guide only with intent for the user to provide his/her own fatigue data for more accurate analysis. In the case of assemblies with different materials, each part will use its own fatigue material properties just as it uses its own static properties (like modulus of elasticity).

Fatigue results can be added before or after a stress solution has been performed. To create fatigue results, a fatigue tool must first be inserted into the tree. This can be done through the solution toolbar or through context menus. The details view of the fatigue tool is used to define the various aspects of a fatigue analysis such as loading type, handling of mean stress effects and more. This can be very useful to help a novice understand the fatigue loading and possible effects of a mean stress. Fatigue, by definition, is caused by changing the load on a component over time. Thus, unlike the static stress safety tools, which perform calculations for a single stress, fatigue damage occurs when the stress at a point changes over time. ANSYS can perform fatigue calculations for either constant amplitude loading or proportional non-constant amplitude loading. A scale factor can be applied to the base loading if desired. This option, located under

the “Loading” section in the details view, is useful to see the effects of different finite element load magnitudes without having to re-run the stress analysis. Several results for evaluating fatigue are available to the user. Some are contour plots of a specific result over the model while others give information about the most damaged point in the model(or the most damaged point in the scope of the result). Outputs include fatigue life, damage, factor of safety, stress biaxiality, fatigue sensitivity, rainflow matrix, and damage matrix output. A contour plot of available life over the model can be find out easily. This result can be over the whole model or scoped to a given part or surface. This result contour plot shows the available life for the given fatigue analysis. If loading is of constant amplitude, this represents the number of cycles until the part will fail due to fatigue. If loading is non-constant, this represents the number of loading blocks until failure. Thus if the given load history represents one month of loading and the life was found to be 120, the expected model life would be 120 months.

A fatigue sensitivity plot shows how the fatigue results change as a function of the loading at the critical location on the model. This result may be scoped to parts or surfaces. Sensitivity may be found for life, damage, or factory of safety. The user may set the number of fill points as well as the load variation limits. For example, the user may wish to see the sensitivity of the model’s life if the load was 50% of the current load up to if the load 150 % of the current load. (The x value of 1 on the graph corresponds to the life at the current loading of the model. The x-value at 1.5 corresponds to the critical fatigue life if the finite element loads were 50 % higher than they are currently.

Chapter 5

Designing and Simulation

5.1 Introduction

Loads and constraints are applied and the solution is then determined by using ANSYS simulation tool. It uses a preprocessor software engine to create geometry. Then it uses a solution routine to apply loads to the meshed geometry. Finally it outputs desired results in post-processing. Different cantilever designs are revealed having fixed thickness of 2 mm, maximum length and breadth of each structure is 26 mm and 17 mm, but the area under different structures is not equal, all these structures have different values for mass and volume. Sensitivity and life of sensor is greatly depended upon shape and size of cantilever structure. So in this present chapter we are emphasizing on different possible designs of cantilevers for slip detecting sensor in prosthetic fingertips, so as to enhance sensitivity and life, while reducing size and weight. Different aspects of each and every shape have been considered like stress, strain and deformation. Simulation results are obtained for different structures at different loading positions. In case of squared frame beam, load is applicable only at one position that is into the centre of beam. Also the impact of (increasing or decreasing) contact area on the stress, strain and deformation values has been analyzed.

5.2 Material properties

Conventionally ceramic materials such as alumina are used. But for this application the production of sensors on an alumina cantilever would be inappropriate since this material is too brittle to withstand the bending forces applied to the fingertips when in use. Fortunately, particular grades of stainless steel have proved to be compatible with the thick film process and have therefore been considered here. Stainless steel also has the additional advantage that it may be machined and shaped more readily than alumina (9).

The cantilevers are machined from grade 304 stainless steel and has a nominal thickness of 2 mm, which may be changed (along with the beam width) to adjust the sensitivity or the measurement range of the device. Physical and mechanical properties of stainless steel are shown in Table 5.1, while the values of strain life parameters are shown in Table 5.2.

Table 5.1 Stainless steel properties

Physical properties	Metric
Density	8.00g/cc
Hardness, Brinell	123
Hardness, Knoop	138
Hardness, Rockwell B	70
Tensile strength, ultimate	505MPa
Tensile strength, Yield	215MPa
Elongation at break	70.0%
Modulus of elasticity	193-200GPa
Poission ratio	0.29
Charpy impact	325j
Shear modulus	86.0GPa

Table 5.2 Strain life parameters of stainless steel

Strain life parameters	Metric
Fatigue Strength Coefficient (MPa)	796MPa
Fatigue Ductility Coefficient	0.425
Fatigue Strength Exponent	-0.129
Fatigue Ductility Exponent	-0.513
Cyclic Strength Coefficient (MPa)	716MPa
Cyclic Strain Hardening Exponent	0.207

5.3 Different possible geometries

Solid modeling in ANSYS workbench can be accomplished in a number of ways, and one favorite method involves starting with a two-dimensional shape and manipulating it to create a solid. That is the approach we will use for many of the object models created in this dissertation. Using ANSYS design modeler the geometry of beam is created with thickness value of 2 mm, two holes of 3 mm diameter are drawn in every structure. Each cantilever structure has different

area and volumes, but the dimensions of maximum length and breadth are fixed such that each structure must be mimics to the shape of human finger. Maximum length and breadth of each cantilever structure does not exceed 26 mm and 17 mm respectively.

1. T-shaped cantilever beam

The designed geometry of the beam is shown in Figure 5.1. The beam with thickness value of 2 mm has been generated, the base root of beam is 6 mm wide and breadth of base root is 17 mm, while the total length of beam is 26 mm. central bar of the beam has a breadth of 7 mm.

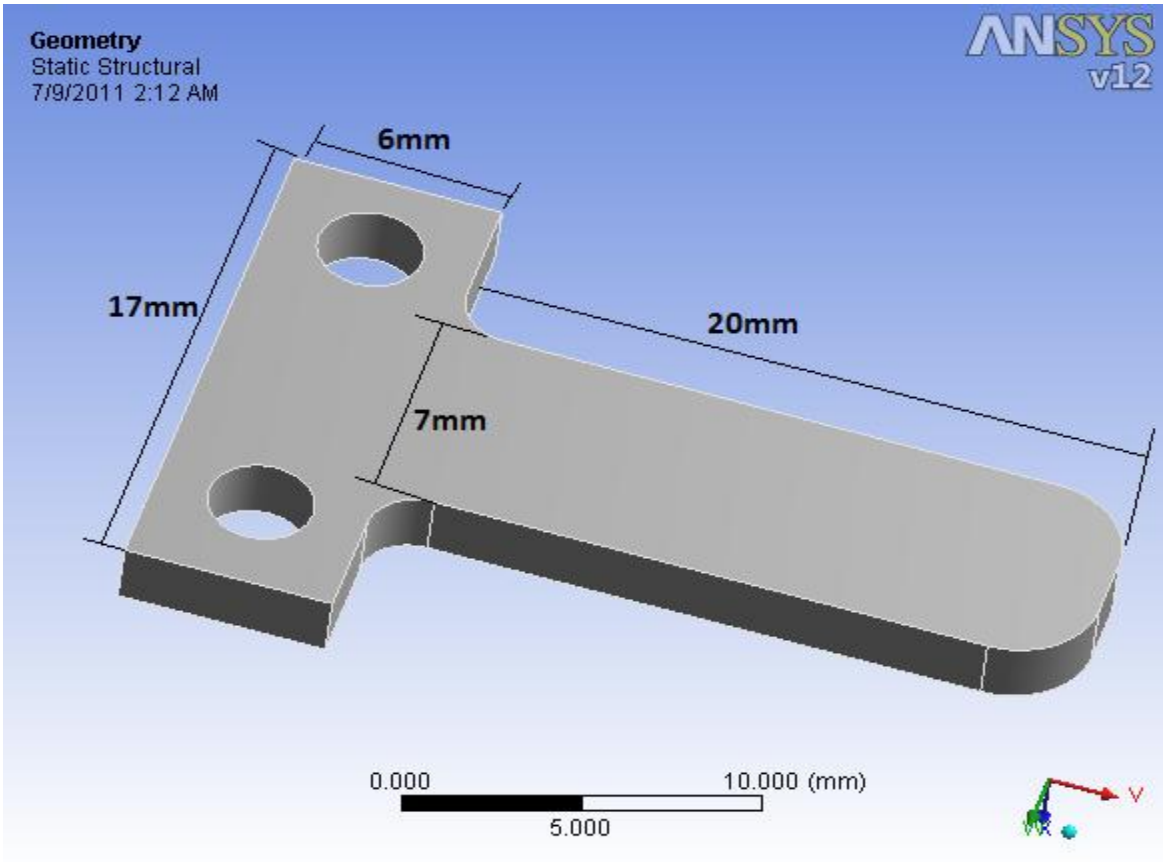

Figure 5.1 T-shaped cantilever beam

2. Rectangular cantilever beam

This beam has nominal value of thickness as 2 mm, length of 26 mm and breadth of 17 mm. there are two holes driven with diameter of 3 mm each. The designed geometry of the beam is shown in Figure 5.2.

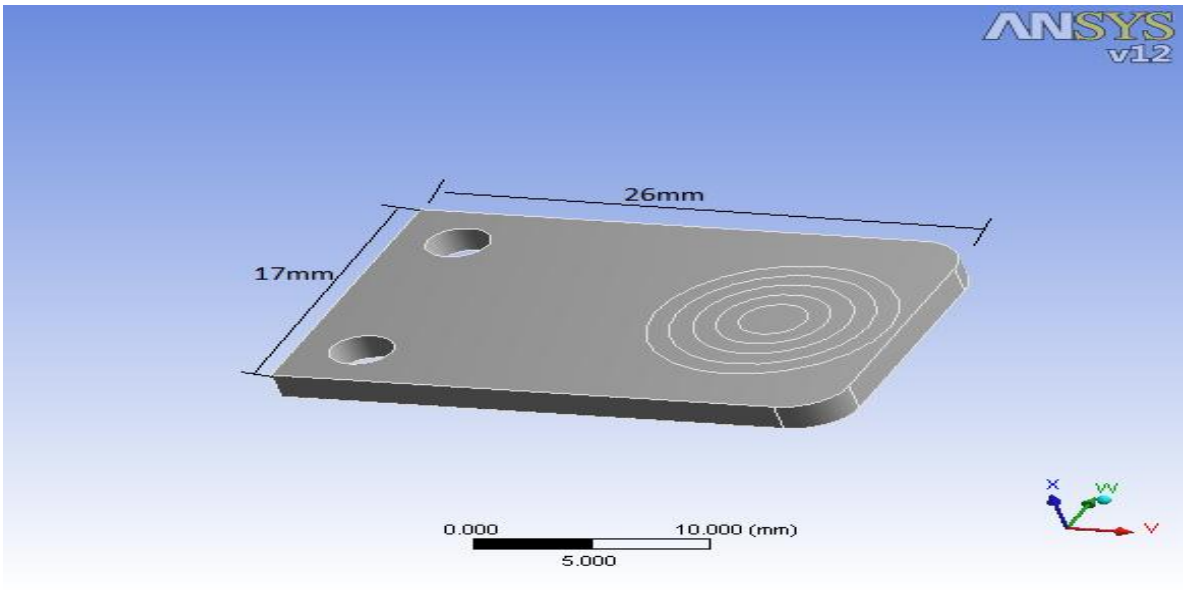

Figure 5.2 Rectangular cantilever beam

3. Tapered cantilever beam

The different dimensions of the tapered cantilever beam are shown in Figure 5.3. The base root of beam is with 17 mm breadth and 6 mm long, while the total length of beam is 26 mm.

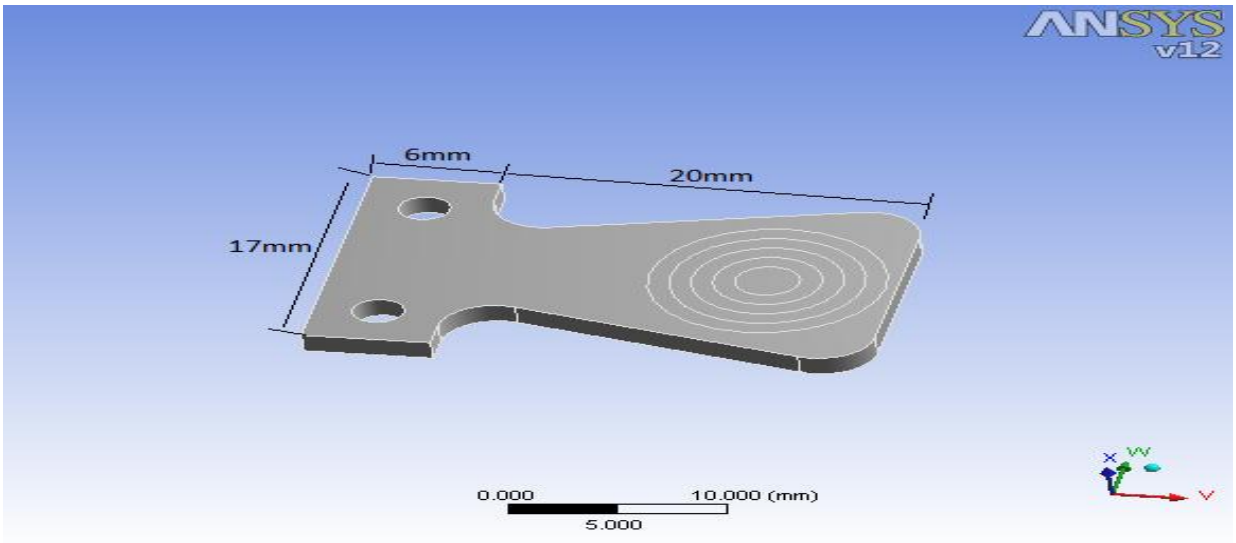

Figure 5.3 Tapered cantilever beam

4. Circular end cantilever beam

Figure5.4 is a circular end cantilever design, the total length of the beam including base root is 26 mm, there is a half circle of 13 mm have been drawn at end of beam.

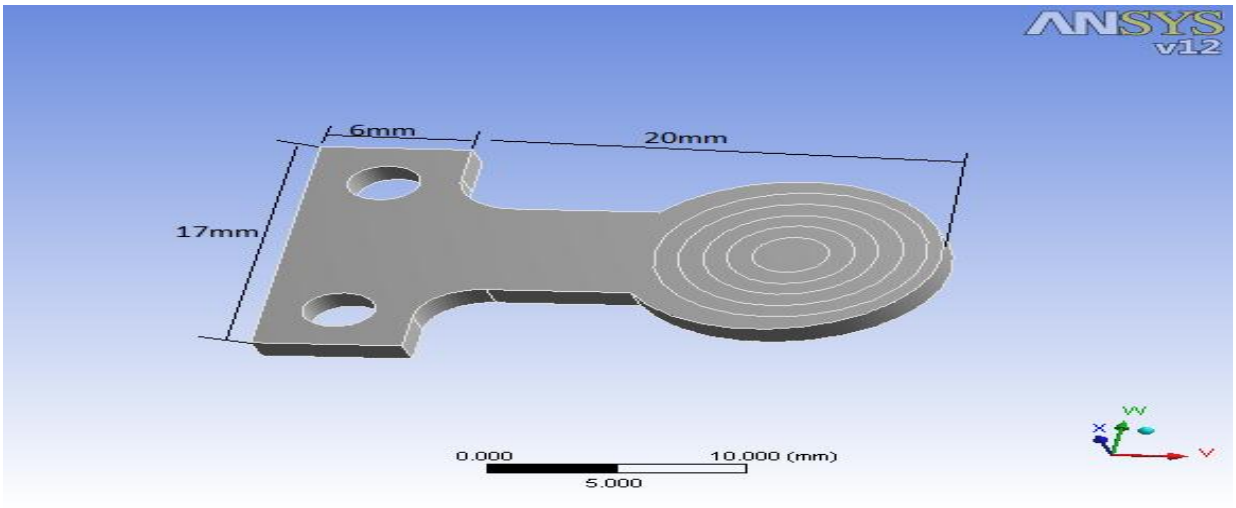

Figure 5.4 Circular end cantilever beam

5. Squared frame cantilever beam

In this case a square of outside edges of 17×17 mm have been drawn with a wall of thickness 3 mm. The central square is of 6×6 mm and a circle of 5 mm has been drawn for the purpose of force application region.

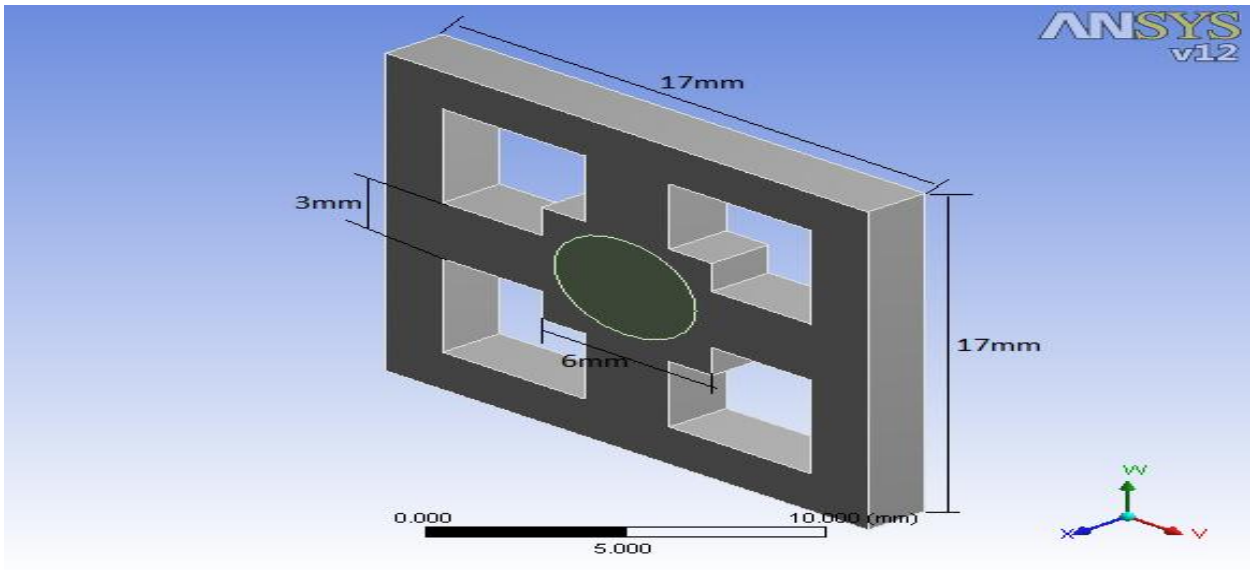

Figure 5.5 Squared frame beam

5.4 Comparison of mass and volume of different geometries

Table 5.3 shows that rectangular geometry has maximum mass and volume, on the other hand squared frame beam is geometry of minimum mass and volume.

Table 5.3 Mass and volume of different structure

Shape	Mass(Kg)	Volume(mm^3)
Rectangular	0.006693	852.64
Tapered	0.005228	665.96
Circular end	0.004359	544.9
Squared	0.003168	396
T-shape	3.62E-03	452.29

5.6 Application of supports

For the purpose of assigning fixed boundary conditions to the different structures the shape of finger in Southampton hand has been clearly revised. As shown in Figure 5.6 below there are two holes driven at fingertip support and one backside wall of 2 mm which is also helpful for providing support to the different shaped cantilever beams except for the squared frame structure which has been just considered as a possible case for any newly discovered fingertip design in which we need four squared walls with a empty space of 17×17 mm in the centre.

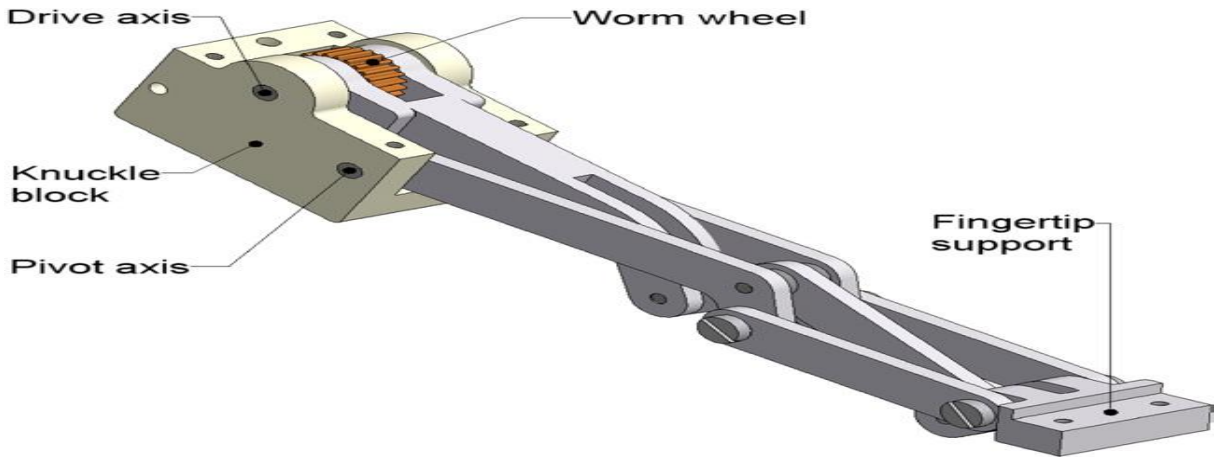

Figure 5.6 Finger of Southampton hand

Supports are the boundary conditions which are necessary to be fixed in the ANSYS workbench for the purpose of simulating different designs. Depending upon the design considerations of

Southampton hand we have assigned different three supports to each tapered, circular end, t-shape and rectangular structures as shown in Figure 5.7, while different four supports are necessary for squared frame structure as shown in Figure 5.8.

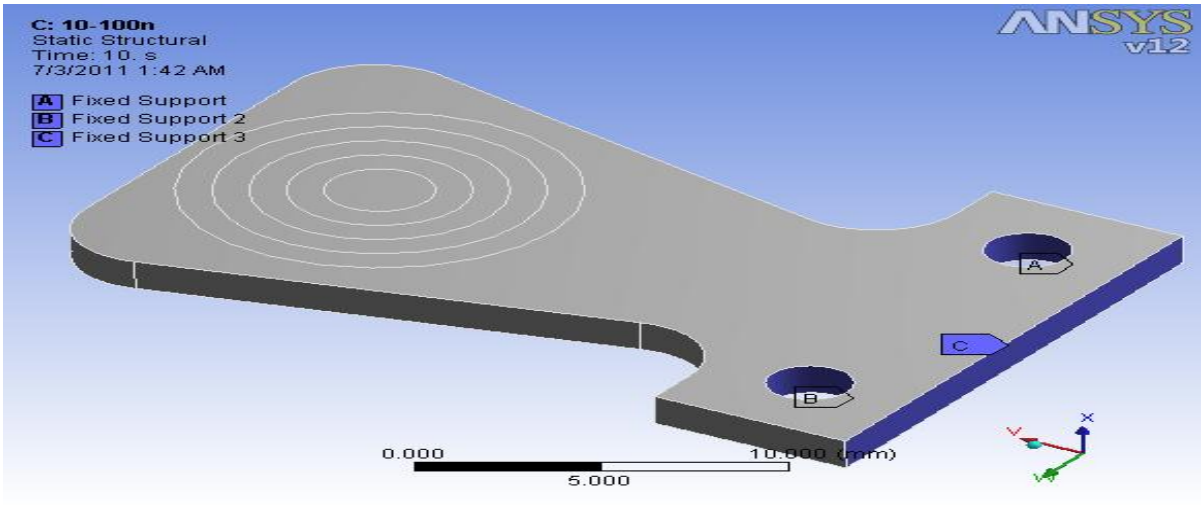

Figure 5.7 Three supports

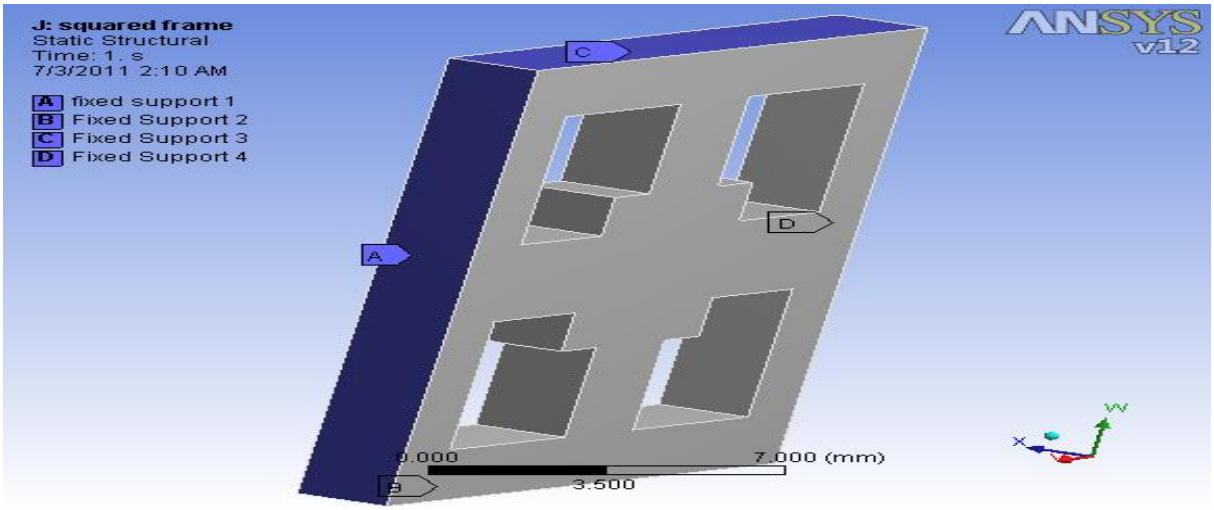

Figure 5.8 Four supports

5.6 Application of load at different positions

After fixing each and every structure, load of 10-100 N is applied on different three positions of each rectangular, t-shape, circular end and tapered cantilever beams. These different positions of load application regions are shown in Figures 5.9, 5.10 and 5.11 for a rectangular cantilever structure. On the other hand due to the different symmetry of squared frame geometry load is applicable only at one position as shown in Figure 5.12.

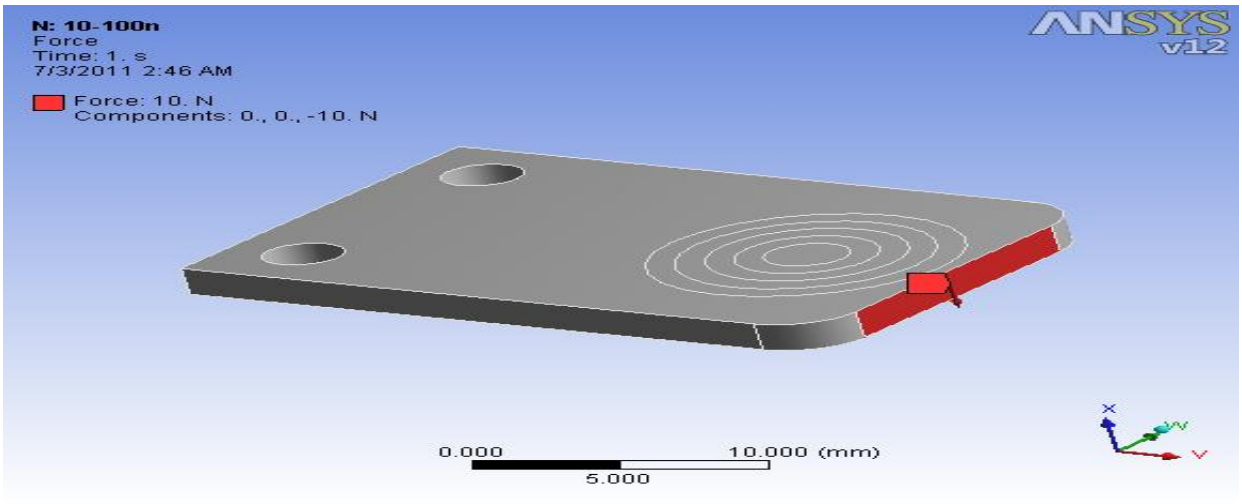

Figure 5.9 Load on end face

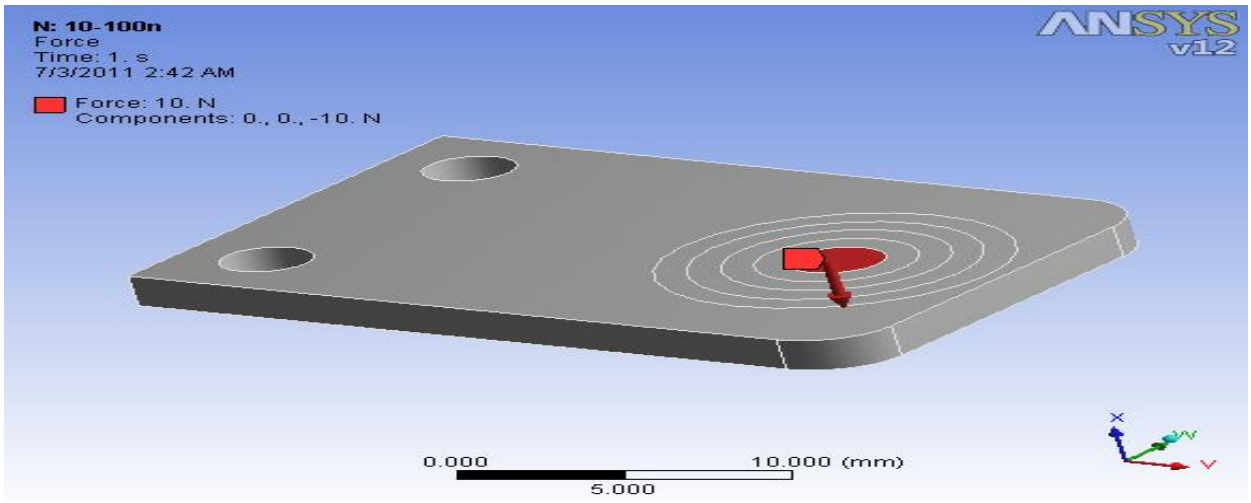

Figure 5.10 Load on front face

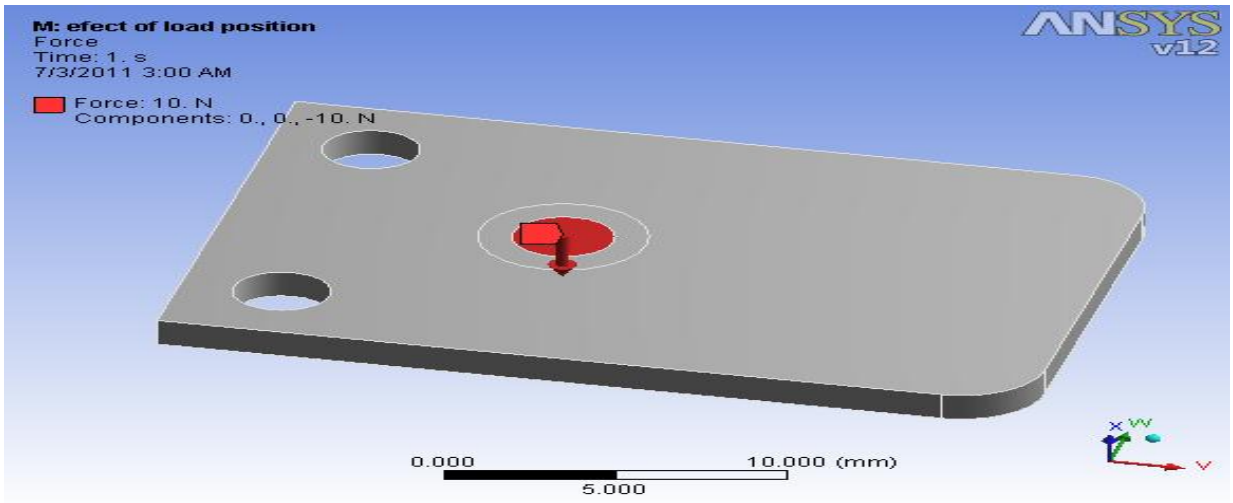

Figure 5.11 Load in centre

It should be noted out that in all the four structures rectangular, circular end, tapered and t-shape there are three different positions possible for the application of load that is load on end face, load on front face, load in the centre as shown above in Figures 5.9, 5.10, 5.11 respectively. But in the case of squared frame structure, load should be applicable only at one position that is into the centre of frame as shown below in Figure 5.12.

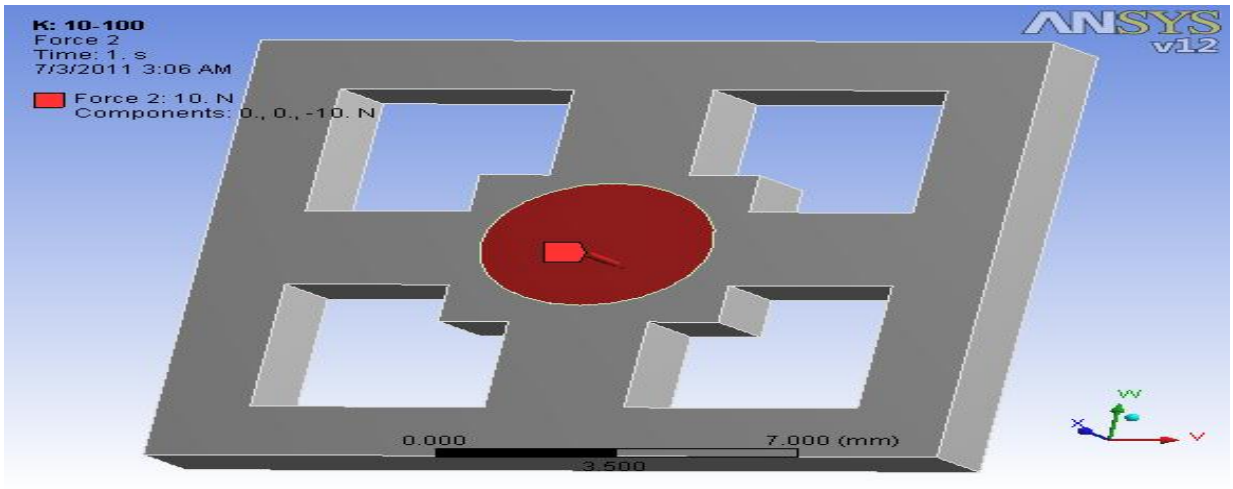

Figure5.12 Load on squared frame beam

5.7 Stress, strain and deformation at different loading position

5.7.1 Introduction

A fundamental premise of using the finite element procedure is that the body is sub-divided into small discrete regions known as finite elements. These elements defined by nodes and interpolation functions. Governing equations are written for each element and these elements are assembled into a global matrix. Once all the requirements of modeling have been full-filled, then we can proceed for the solution routine. During simulation we have applied different forces from 10-100 N on each structure and the corresponding generation of maximum and minimum values of stress, strain and deformation have been calculated. Application of load on different positions produced significant effects on stress, strain and deformation values.

5.7.2 Load on end face

Application of load on end face is a method of analyzing the maximum changes in geometry of cantilever beam, application of load is done as shown in Figure 5.9. Application of load produces

strain, stress and deformation.

A. Production of strain

Simulation result for strain production in tapered cantilever beam has been shown in Figure 5.13.

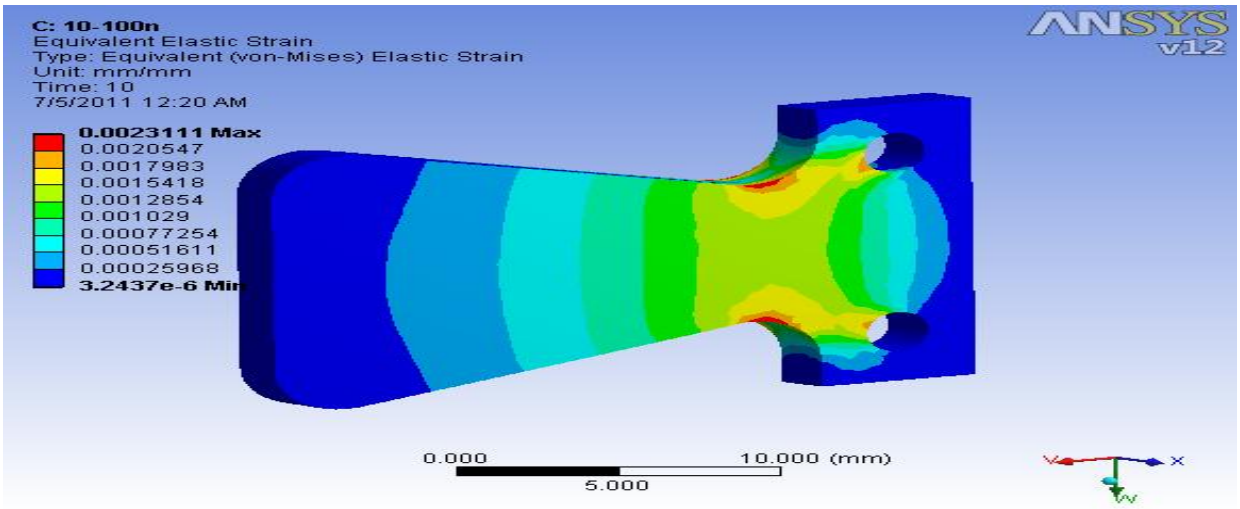

Figure 5.13 Strain in tapered beam

Table 5.4 shows the simulation results for change in strain for different structures at different forces from 10-100 N. Results are obtained for a case in which load acts on end face of the beam.

Table5.4 Changes in strain for end face loading

Force(N)	Circular end	Rectangular	T-shape	Tapered
10	1.85609103E-4	1.7450043E-4	0.00032607	2.3078563E-4
20	3.7121821E-4	3.4899086E-4	0.00065213	4.6158126E-4
30	5.5682731E-4	5.2349129E-4	0.00097820	6.9236689E-4
40	7.4243641E-4	6.9799172E-4	0.00130426	9.231525E-4
50	9.2804551E-4	8.7249215E-4	0.00163035	0.0011539781
60	0.00111369462	0.0010470226	0.00195644	0.0013847538
70	0.00129924372	0.001221443	0.00228243	0.0016155294
80	0.00148489282	0.0013959634	0.00260852	0.001846305
90	0.00167044193	0.0015704839	0.00293461	0.0020770807
100	0.00185609103	0.0017450043	0.00326070	0.0023078563

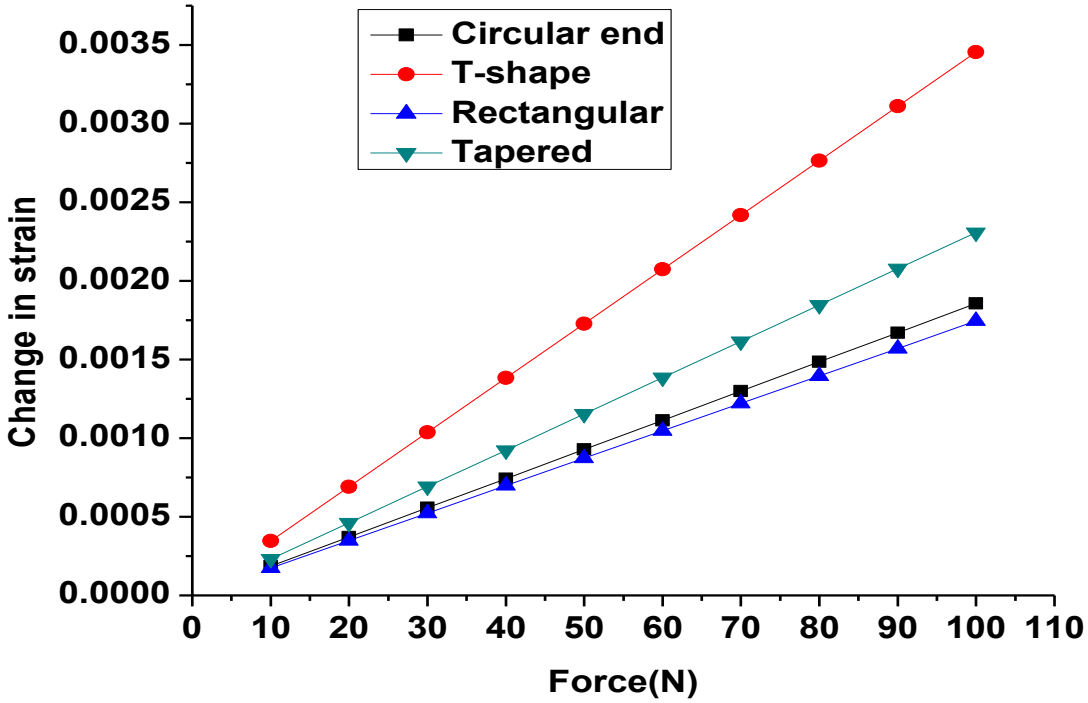

Figure 5.14 Force v/s changes in strain for end face load

A graph has been plotted for strain change when load is on end face at different forces as shown in Figure 5.14, and it clearly indicates that maximum changes in strain comes for T-shape structure while rectangular shape is with minimum production of strain.

B. Production of stress

For the same case when load is applied on end face, the simulation results for stress production have been analyzed for different four structures. Table 5.5 shows the changes in stress that is difference between maximum and minimum values of stress at different forces from 10-100 N for different possible shapes of cantilever beams. These are the values obtained for a case when load acts on end faces of the beams.

A graph has been plotted for the values of change in stress given in Table 5.5, by taking force from 10-100 N along X-axis and change in stress (MPa) along Y-axis. It is clearly indicated by the graph that T-shape structure is maximum sensitive to load while minimum change in values of stress comes across rectangular structure.

Table 5.5 Changes in stress for end face loading

Force(N)	Tapered	Circular end	T-shape	Rectangular
10	44.5424	35.82218	62.9311533	33.67834
20	89.08479	71.64535	125.8663065	67.35669
30	133.62219	107.47053	188.7944598	101.03603
40	178.16959	143.29071	251.722613	134.71137
50	222.70698	179.11088	314.6507663	168.38672
60	267.25438	214.93106	377.58892	202.07206
70	311.79178	250.76124	440.517073	235.7474
80	356.33917	286.58141	503.445226	269.42274
90	400.87657	322.40159	566.373379	303.09809
100	445.42396	358.22177	629.311533	336.78343

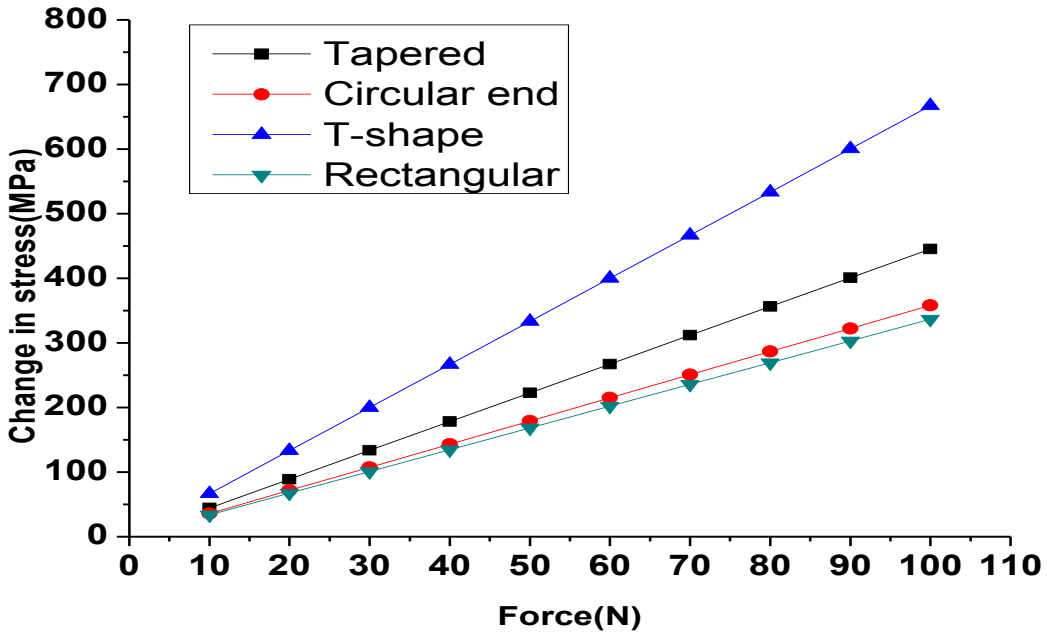

Figure 5.15 Force v/s changes in stress for end face load

C. Deformation

When force is applied on any type of solid geometry it gets slightly deformed depending upon force, strength, size and shape of material different deformation parameters should be obtained.

Here we are considering deformation values just to analyze their dependency on shape. Simulation results have been obtained as shown in Figure 5.16, when load is on end face.

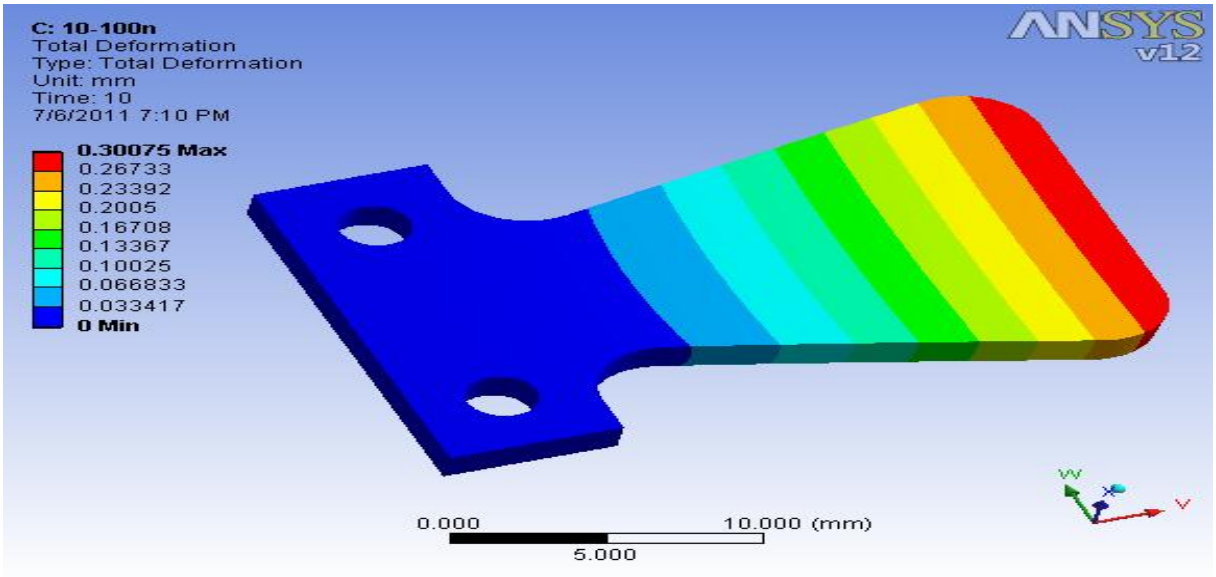

Figure5.16 Deformation for end face load

Table 5.6 shows the different values of deformation (mm) for four different shapes when load is on end face. End face loading is a case in which maximum deformation in each of the four structures is possible.

Table 5.6 Deformation at different forces

force(N)	Rectangular	Circular end	T-shape	Tapered
10	0.0169	0.0249	3.99E-02	0.0301
20	0.0338	0.0499	7.99E-02	0.0602
30	0.0507	0.0748	0.11982	0.0902
40	0.0676	0.0998	0.15976	0.1203
50	0.0845	0.12473	0.1997	0.15037
60	0.10145	0.14967	0.23964	0.18045
70	0.11835	0.17462	0.27957	0.21052
80	0.13526	0.19956	0.31951	0.2406
90	0.15217	0.22451	0.35945	0.27067
100	0.16908	0.24945	0.39939	0.30075

Graph has been plotted for different structures with a changing force of 10-100 N taken along X-axis and deformation (mm) taken along Y-axis as shown in Figure 5.17. T-shape cantilever beam is maximum deformed structure while rectangular beam is a minimum deformed structure.

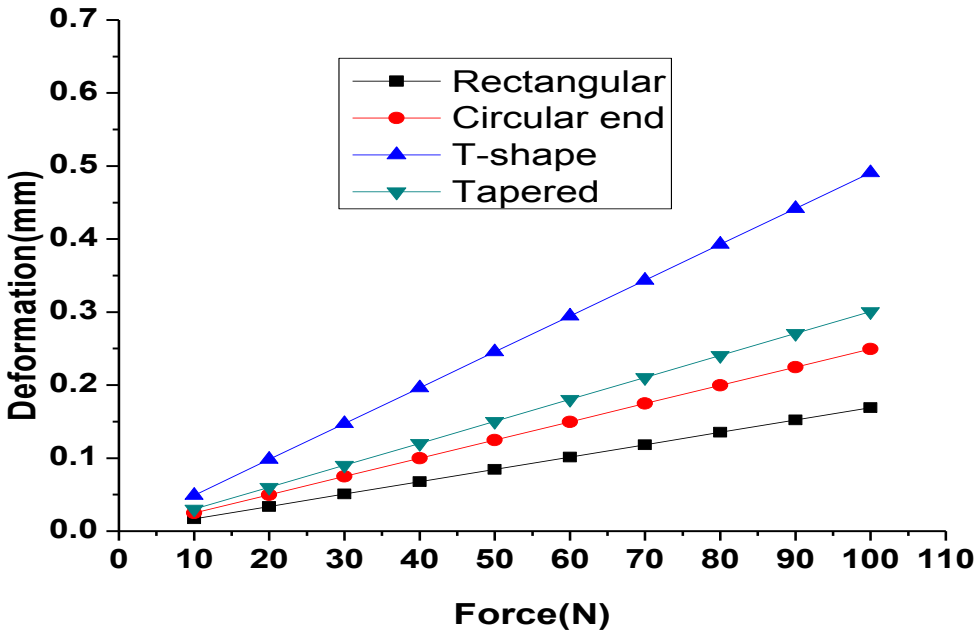

Figure 5.17 Deformation v/s force for end face load

5.7.3 Load on front face

In this case load is applied on front face of cantilever beam. Although for testing or analyzing stress-strain characteristics normally load is applied on end tip of cantilever beam, but for our purpose of slip detection the practical application of load should be on front face. So we have assumed that the fingertip location of cantilever beam should be 20 mm away from root of the beam. So In this case we have applied force from 10-100 N in a circle of diameter 3 mm on the front face of all the different structures as shown in Figure 5.10, except for a case of squared frame beam where load is applied on maximum possible area of circular region with a diameter of 5 mm as shown in Figure 5.12.

A. Strain production

Application of load from 10-100 N on different structures produces different amount of strain.

Simulation results for one of the different structures have been shown below in Figure 5.18. It should be noted out that the centre of force is 20 mm away from the beam roots, but in case of squared frame beam the only possibility is to apply load in Central Square of 6×6 mm by plotting circle of 5 mm diameter on it as shown in Figure 5.12.

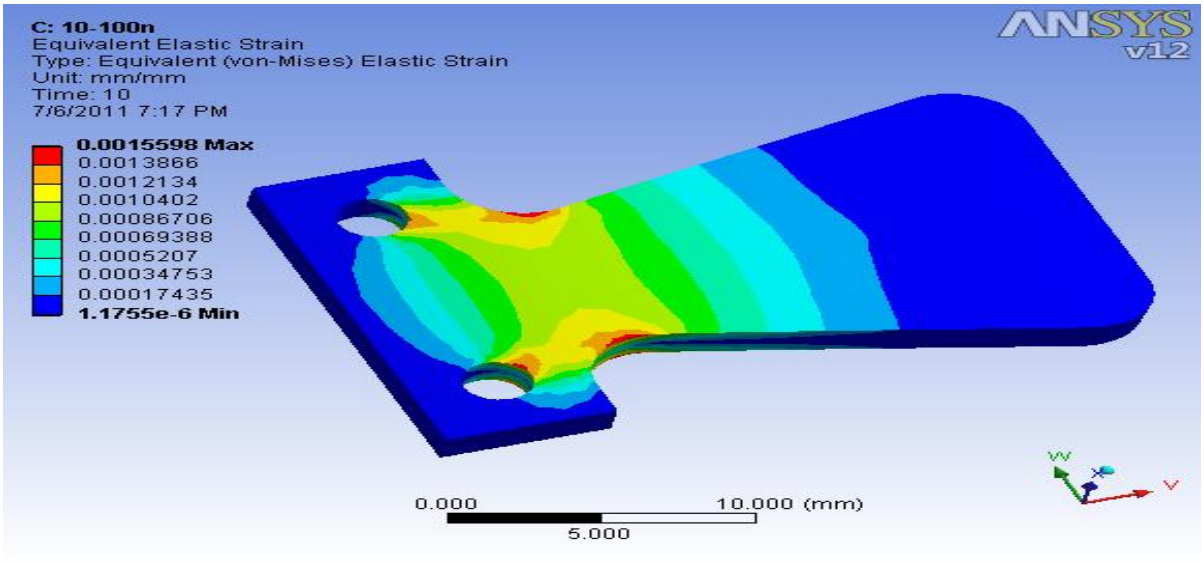

Figure5.18 Strain for front face load

Table 5.7 shows all the values of change in strain for all the different structures at force from10-100 N when load is on front face at a distance of 20 mm away from the base beam of cantilever.

Table 5.7 Changes in strain for front face loading

Force(N)	Rectangular	Circular end	Tapered	T-shape	Squared
10	1.27554E-4	1.7223E-4	1.55862E-4	0.000224659749	2.04088E-5
20	2.55108E-4	3.44461E-4	3.11715E-4	0.000449319499	4.08186E-5
30	3.82662E-4	5.16681E-4	4.67577E-4	0.000673979248	6.12275E-5
40	5.10217E-4	6.88911E-4	6.2343E-4	0.000898638997	8.16363E-5
50	6.37771E-4	8.61142E-4	7.79292E-4	0.001123348747	1.02044E-4
60	7.65335E-4	0.00103	9.35155E-4	0.001347938496	1.22453E-4
70	8.92889E-4	0.00121	0.00109	0.001572628245	1.42862E-4
80	0.00102	0.00138	0.00125	0.001797317995	1.63271E-4
90	0.00115	0.00155	0.0014	0.002021907744	1.83679E-4
100	0.00128	0.00172	0.00156	0.00224659749	2.04088E-4

A graph has been plotted for the obtained values of change in strain at different forces as shown in Figure 5.19. It should be easily predicted that maximum change in strain comes for T-shape structure while squared frame beam is with lowest values of change in strain.

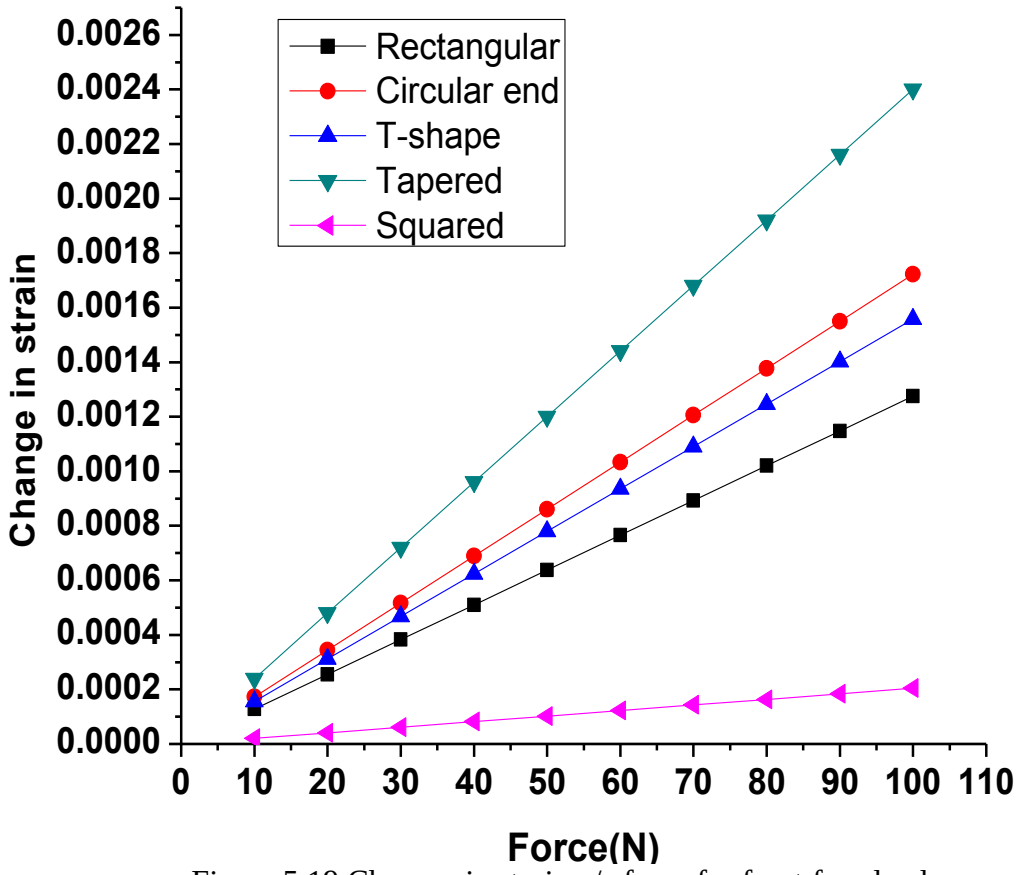

Figure 5.19 Changes in strain v/s force for front face load

B. Stress production

Simulation results of change in stress (MPa) when load is applied on front face of all the beams have been obtained. Table 5.8 shows the change in values of stress (MPa) for all the five structures when forces from 10-100 N are applied.

A graph is plotted for the values obtained as shown in Figure 5.20 for front face loading. Here force from 10-100 N is taken along X-axis while changes in stress (MPa) values have been taken along Y-axis. T-shape structure is with maximum values of stress change while squared frame has minimum sensitivity for different loads.

Table 5.8 Changes in stress for front face loading

Force(N)	Tapered	Squared	Circular end	Rectangular	T-shape
10	30.08031	3.93897	33.24041	24.61764	43.3590216
20	60.16163	7.87795	66.47983	49.23629	86.7190432
30	90.24194	11.81732	99.72024	73.85393	130.0740649
40	120.31925	15.75609	132.96165	98.47257	173.4420865
50	150.40656	19.69486	166.20207	123.08821	216.8001081
60	180.48388	23.63364	199.44248	147.70585	260.15813
70	210.56119	27.57241	232.68289	172.3235	303.516151
80	240.6485	31.51118	265.92331	196.94114	346.874173
90	270.72582	35.45096	299.16372	221.55878	390.232195
100	300.80313	39.38973	332.40413	246.17642	433.590216

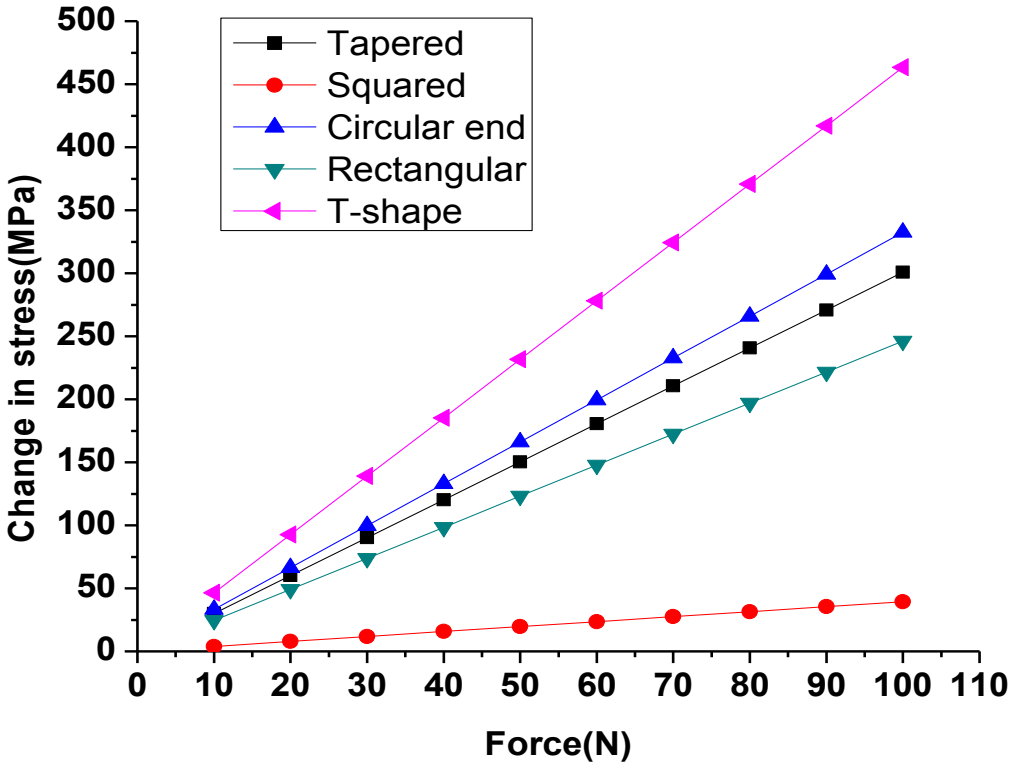

Figure 5.20 Variation of stress v/s force in front face load

C. Deformation

Table 5.9 shows the simulation results of deformation (mm) at different forces from 10-100 N for front face loading.

Table 5.9 Deformation when load is on front face

Force(N)	Rectangular	Tapered	Circular end	T-shape	Squared
10	0.01033	0.01875	0.02268	2.41E-02	2.094E-4
20	0.02065	0.0375	0.04536	4.82E-02	4.188E-4
30	0.03098	0.05624	0.06804	7.23E-02	6.282E-4
40	0.0413	0.07499	0.09072	9.65E-02	8.376E-4
50	0.05163	0.09374	0.1134	0.12058	0.00105
60	0.06196	0.11249	0.13608	0.14469	0.00126
70	0.07228	0.13124	0.15876	0.16881	0.00147
80	0.08261	0.14998	0.18144	0.19293	0.00168
90	0.09293	0.16873	0.20412	0.21704	0.00188
100	0.10326	0.18748	0.2268	0.24116	0.00209

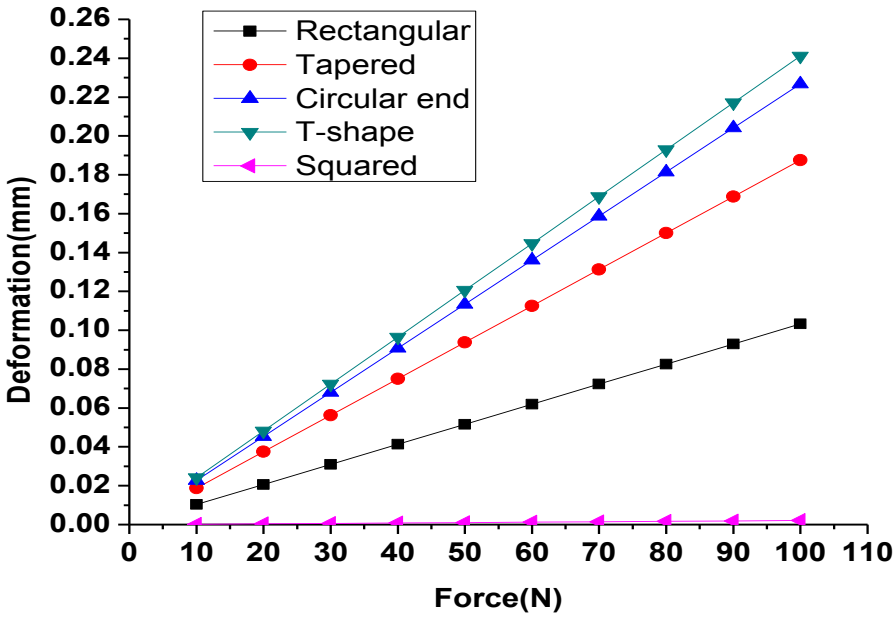

Figure 5.21 Deformation v/s force for front face load

Graph is being plotted for the deformation (mm) values at different forces for all the five structures as shown in Figure 5.21. T-shape structure is with maximum values of deformation, while minimum deformed shape is squared frame beam.

5.7.4 Halfway load on front face

In this case centre of force that is 20 mm away from root of the beam in previous case is shifted to 10 mm on the same face as shown in Figure 5.11. The diameter of circular area of force application region is same that is 3 mm. Again for this position values of strain, stress and deformation have been obtained. Need for analysis at this position arises because our purposes of making these designs are for investigating more efficient sensors for slip and force detection in prosthetic hands. Now its necessary that we must analyze but amount of changes in stress, strain and deformation takes place if centre of force on the cantilever beam is shifted to midway position.

A. Strain production

Simulation results for this case where load is on front face with centre of force 10 mm away from root of beam has been obtained at different forces from 10-100 N as shown in Table 5.10.

Table 5.10 Changes in strain for halfway loading on front face

Force(N)	Rectangular	Tapered	Circular end	T-shape
10	5.44833E-5	6.52203E-5	6.29576E-5	0.0000561105168
20	1.08963E-4	1.30443E-4	1.25917E-4	0.0001122170337
30	1.63454E-4	1.95659E-4	1.88876E-4	0.0001683355505
40	2.17935E-4	2.60875E-4	2.51835E-4	0.0002244440674
50	2.72416E-4	3.26101E-4	3.14793E-4	0.0002805525842
60	3.26898E-4	3.91318E-4	3.77752E-4	0.0003366611011
70	3.81379E-4	4.56544E-4	4.407E-4	0.000392779618
80	4.3586E-4	5.2176E-4	5.03659E-4	0.000448888135
90	4.90351E-4	5.86976E-4	5.66618E-4	0.000504996652
100	5.44833E-4	6.52203E-4	6.29576E-4	0.000561105168

Figure 5.22 indicates the variation of change in strain with different forces from10-100 N for a case where load is at midway on front face. Force (N) is taken along X-axis, while change in strain is taken along Y-axis. Tapered beam structure is with maximum values of change in strain, while rectangular shape is with minimum values of strain changes.

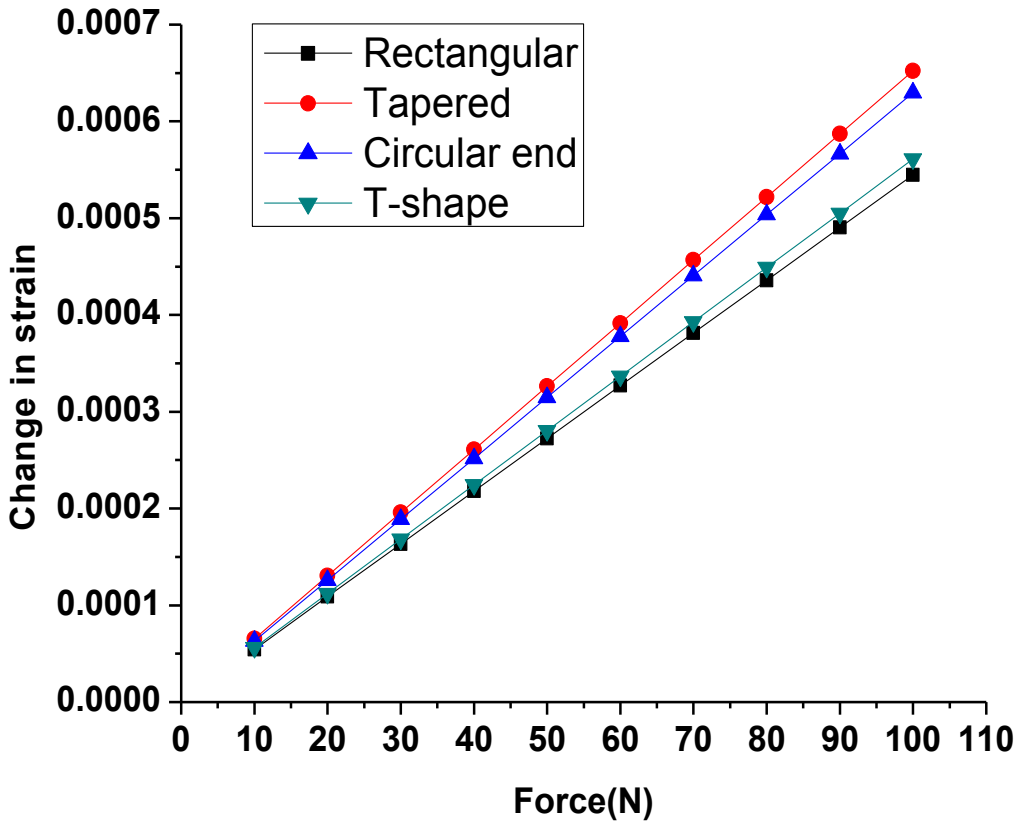

Figure 5.22 Changes in strain v/s force for halfway loading on front face

B. Stress production

Table 5.11 shows the values of change in stress (MPa) obtained after simulation for a case of halfway load on front face at different forces from 10-100 N.

A graph has been plotted for the obtained values in as shown in Figure 5.23, where change in stress (MPa) is taken along Y-axis and force (N) is taken along X-axis. Graph clearly indicates that tapered beam structure is with maximum values of stress changes, while rectangular beam is with lowest values of stress changes.

Table 5.11 Changes in stress for halfway loading on front face

Force(N)	Tapered	Rectangular	T-shape	Circular end
10	12.58728	10.51531	10.82971375	12.15074
20	25.17456	21.03063	21.6584275	24.30147
30	37.76183	31.54595	32.48814125	36.45221
40	50.35011	42.06126	43.317855	48.60395
50	62.93739	52.57657	54.1465688	60.75468
60	75.52466	63.09189	64.9762825	72.90542
70	88.11194	73.6072	75.8059963	85.05616
80	100.70422	84.12152	86.63471	97.20689
90	113.2835	94.63684	97.4644238	109.35763
100	125.87278	105.15315	108.2971375	121.50737

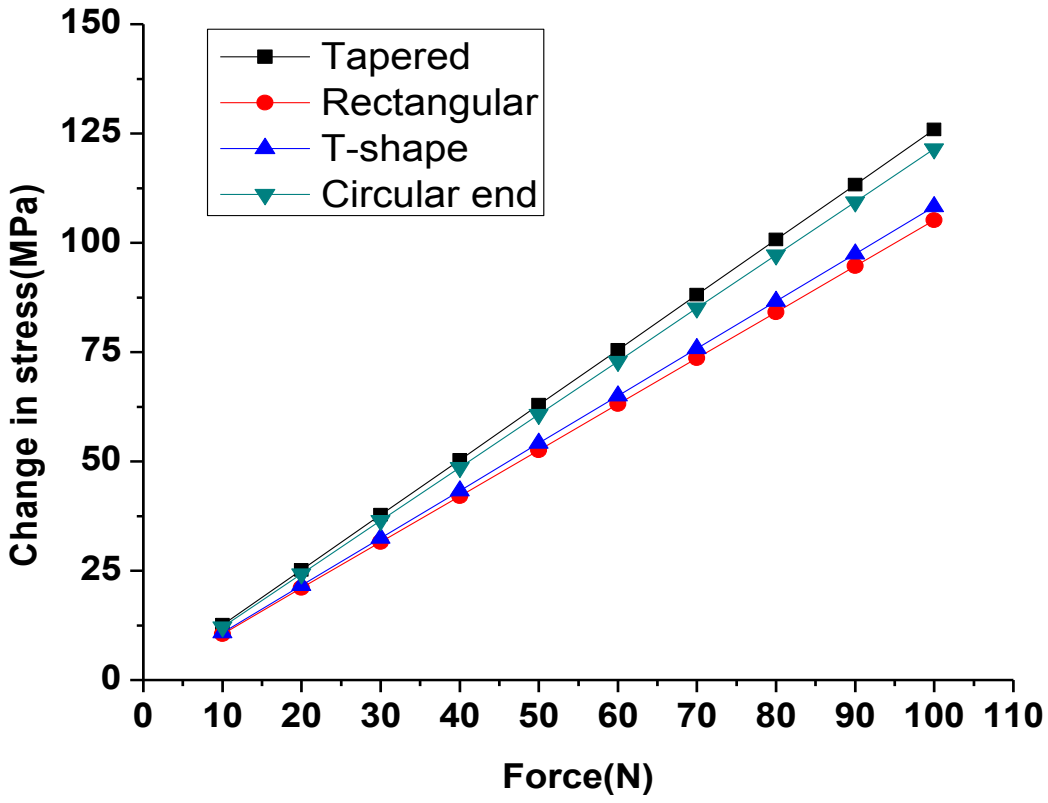

Figure 5.23 Change in stress v/s force for halfway loading on front face

C. Deformation

When we shift the centre of force from 20 mm to 10 mm as shown in Figure 5.12, there are significant decrements in the values of deformation were observed. Table 5.12 contains all the different values of deformation (mm) for four of the structures at forces from 10-100 N.

Table 5.12 Deformation for halfway loading on front face

Force(N)	Rectangular	Circular end	Tapered	T-shape
10	0.00204	0.00415	0.00378	4.29E-03
20	0.00408	0.00831	0.00756	8.58E-03
30	0.00612	0.01246	0.01134	1.29E-02
40	0.00816	0.01662	0.01512	1.72E-02
50	0.01021	0.02077	0.01891	2.15E-02
60	0.01225	0.02492	0.02269	2.58E-02
70	0.01429	0.02908	0.02647	3.00E-02
80	0.01633	0.03323	0.03025	3.43E-02
90	0.01837	0.03739	0.03403	3.86E-02
100	0.02041	0.04154	0.03781	4.29E-02

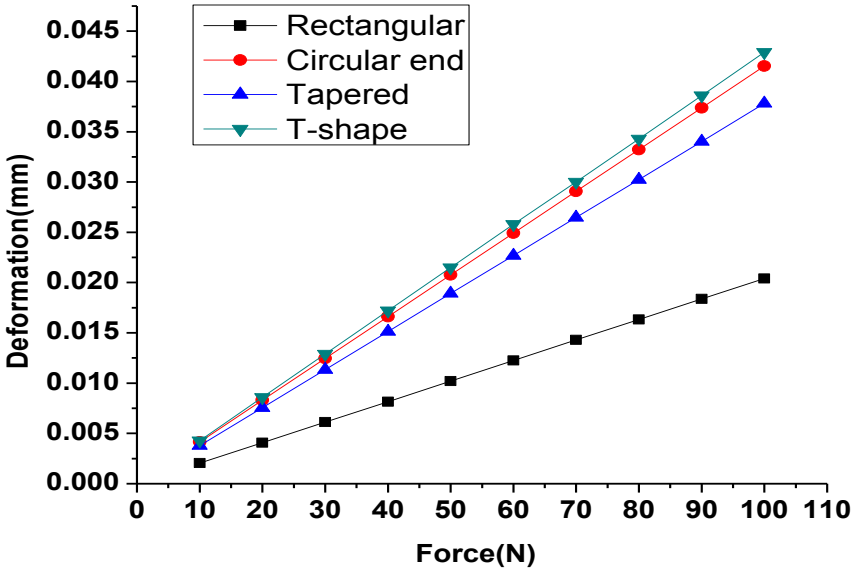

Figure 5.24 Deformation v/s force for halfway loading on front face

Graph is being plotted for deformation (mm) values v/s force for halfway loading on front face as shown in Figure 5.24. T-shape beam is maximum deformed structure while rectangular shape is lowest deformed shape.

5.8 Effects of changing contact area

Effects of changing area of the circular contact region are being studied. If the centre of force remains at same distance for example at 20 mm away from root of the beam as shown in Figure 5.10 and the area of the circular contact region has been increased upto maximum possible dimensions as shown below in Figure 5.25. after that the effects of changing this area has been studied for one of the different structures, and results show that the changes that takes place in the values of stress, strain and deformation are negligible.

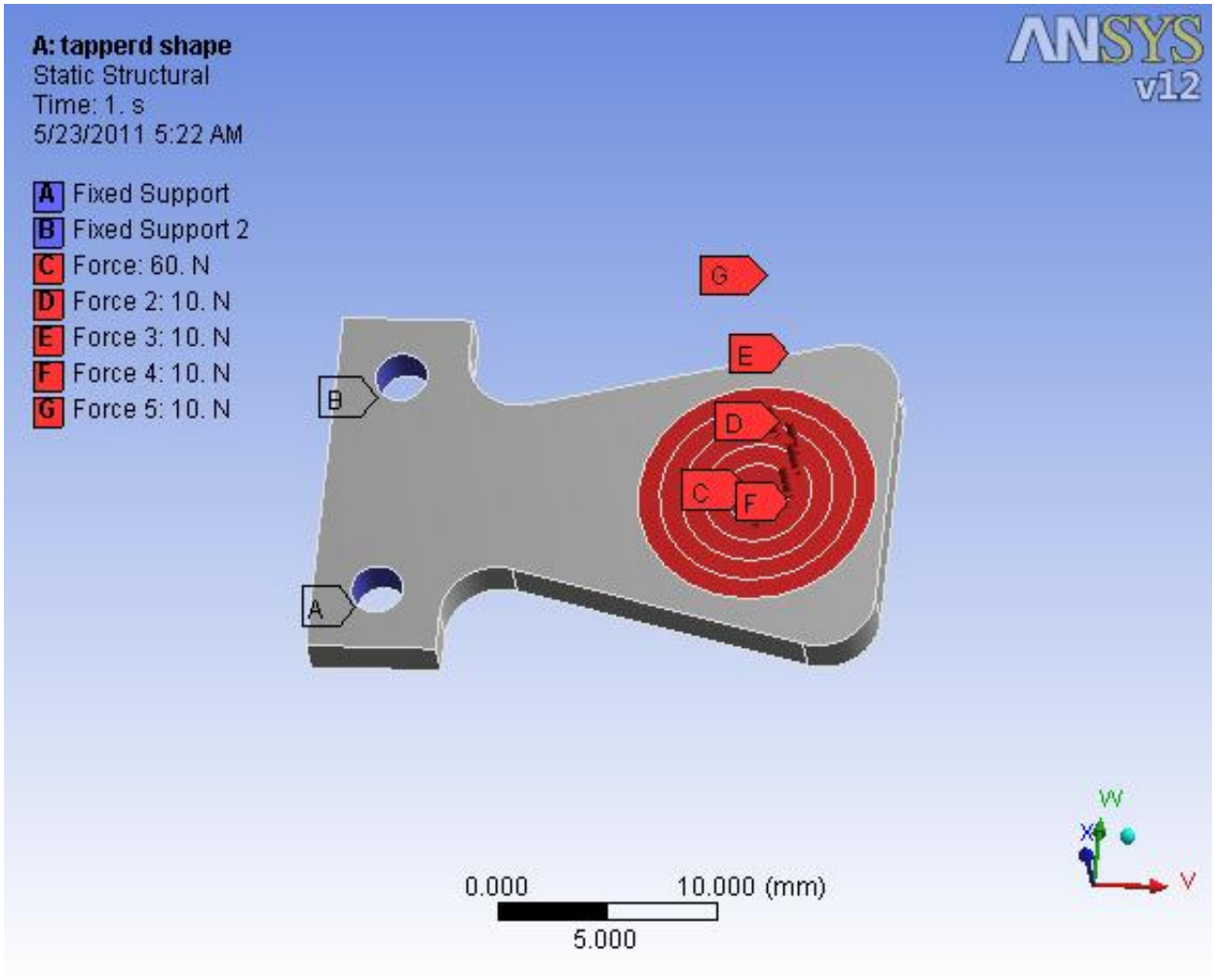

Figure5.25 Load on maximum possible circular area

Table 5.13 gives the simulation results for stress, strain and deformation. These results are obtained by applying load on maximum possible area as shown in Figure 5.25 for a tapered cantilever beam.

Table 5.13 Different values at maximum possible circular contact regions

Force (N)	Change in strain	Change in stress (MPa)	Deformation (mm)
10	0.00015585	30.079649	1.88E-02
20	0.0003117	60.158299	3.77E-02
30	0.00046755	90.237948	5.65E-02
40	0.00062341	120.320597	7.53E-02
50	0.000779261	150.393246	9.41E-02
60	0.000935111	180.4759	0.11298
70	0.001090971	210.55854	0.13181
80	0.001246781	240.63119	0.15064
90	0.001402691	270.71384	0.16947
100	0.001558501	300.79649	0.1883

Results obtained in a Table 5.13 are compared with stress, strain and deformation results of the same beam (tapered) when load in central circle of diameter 3 mm being applied.

Table 5.14 indicates the difference in corresponding values of strain, stress and deformation when load is applied in central circle of 3 mm and secondly when load is applied on maximum possible area. Firstly values of stress, strain and deformation have been obtained for case a case when the area of contact region is maximum these values are shown in Table 5.13. After that these values are subtracted from a case when contact region is a central circle of diameter 3mm. It has been clearly observed that effect of increasing or decreasing contact region on stress, strain and deformation is negligible. So we are not considered this effect in our design purpose, that's why we have analyzed all the structures just under the assumption that centre of force should be at a fixed distance in all the structures, because even a small change in that distance may generate significant changes in values of stress, strain and deformation.

Table 5.14 Difference in values due to changing contact region

Force(N)	Strain change	Stress change (MPa)	Deformation variation(mm)
10	1.18999999999922E-08	0.000661000000000911	-0.0000800000000000002
20	1.48000000000053E-08	0.00333100000000286	-0.00016
30	2.66999999999976E-08	0.00399199999999666	-0.00025
40	1.95999999999617E-08	-0.00134700000000976	-0.000328999999999996
50	3.15000000000081E-08	0.0133140000000083	-0.000408999999999993
60	4.43999999999618E-08	0.00798000000000343	-0.00048999999999999
70	-9.70699999999899E-07	0.00265000000001692	-0.000570000000000015
80	3.21920000000012E-06	0.017310000000009	-0.000659999999999994
90	-2.69089999999994E-06	0.0119799999999941	-0.000740000000000018
100	1.49900000000007E-06	0.00664000000000442	-0.000819999999999987

It is clear from the Table 5.14 that the effects of changing contact area are negligible on the values of strain, stress and deformation.

Chapter 6

Strain and stress life of different designs

6.1 Introduction

It is estimated that 50-90 % of structural failure is due to fatigue, thus there is a need for quality fatigue design tools. The focus of fatigue in ANSYS is to provide useful information to the design engineer when fatigue failure may be a concern. A stress-life approach has been adopted for conducting a fatigue analysis. Several options such as accounting for mean stress and loading conditions are available. Fatigue results can be added before or after a stress solution has been performed. Fatigue, by definition, is caused by changing the load on a component over time. Thus, unlike the static stress safety tools, which perform calculations for a single stress, fatigue damage occurs when the stress at a point changes over time. ANSYS can perform fatigue calculations for either constant amplitude loading or proportional non-constant amplitude loading. To create fatigue results, a fatigue tool must first be inserted into the tree. This can be done through the solution toolbar or through context menus. The details view of the fatigue tool is used to define the various aspects of a fatigue analysis such as loading type, handling of mean stress effects and more. We are limited to fatigue sensitivity analysis of all the different structures of cantilever beam in our current approach of fatigue identification. It should be noted that all the fatigue results in this chapter are being obtained for a case when load is on end face of the beam, because in this position of loading the each geometry of cantilever beam gets deformed to the maximum extent.

6.2 Approach for fatigue analysis

For the purpose of fatigue analysis a single case is taken, where load is applied on end face of the beam as shown in Figure 5.9. Because this is a case when there are maximum deformations or disturbances in all the type of cantilever beams take place. But approach of load application in case of squared frame beam remains as before, where only one case of load application position is possible as shown in Figure 5.12. Different curves of fatigue sensitivity have been obtained. It should be noted that there are two cases possible (stress and strain) for analyzing fatigue sensitive behavior of different designs.

1. Strain life

In this case the ANSYS workbench use strain life parameters of material and plot the life of strain versus percentage of applied force (100 N) from 50-150 %.

2. Stress life

Different materials have different life of stress, it is significantly affected by shape of the design. Mean and alternating values of stress are included in engineering data of ANSYS workbench. Then fatigue sensitivity curves have been obtained which contains life along y-axis and percentage of applied force (100 N) from 50-150 % along x-axis.

6.3 Life of different designs

6.3.1 Introduction

Strain life curves are obtained for different structures. It has been assumed that the infinite life of each design is 600 months. After fixing these parameters the fatigue sensitive curves are obtained firstly for strain life and then for stress life which shows the life of design along y-axis and percentage of applied force (100 N) from 50-150 % is taken along x-axis. In all the structures load has been applied at a position which generates maximum deformation, and that is possible for a case when load is on end face as shown in Figure 5.9.

6.3.2 Strain life curves

These curves convey the information of strain life of different designs. The impacts of increasing or decreasing the magnitude of force on strain life of different designs have been studied. For this purpose the ANSYS workbench use strain life parameters of material and plot the curves which shows life of strain versus percentage of applied force (100 N) from 50-150 %.

1. Tapered cantilever beam

ANSYS simulation result for this shape has been shown in Figure 6.1. It will be easily predictable from this graph that the design does not lose its strain life of 600 months up to a force of 95 N, but after this limit of load our structure of cantilever beam starts to lose strain life. Minimum life of strain associated with it is 142 months that is under a load of 150 N.

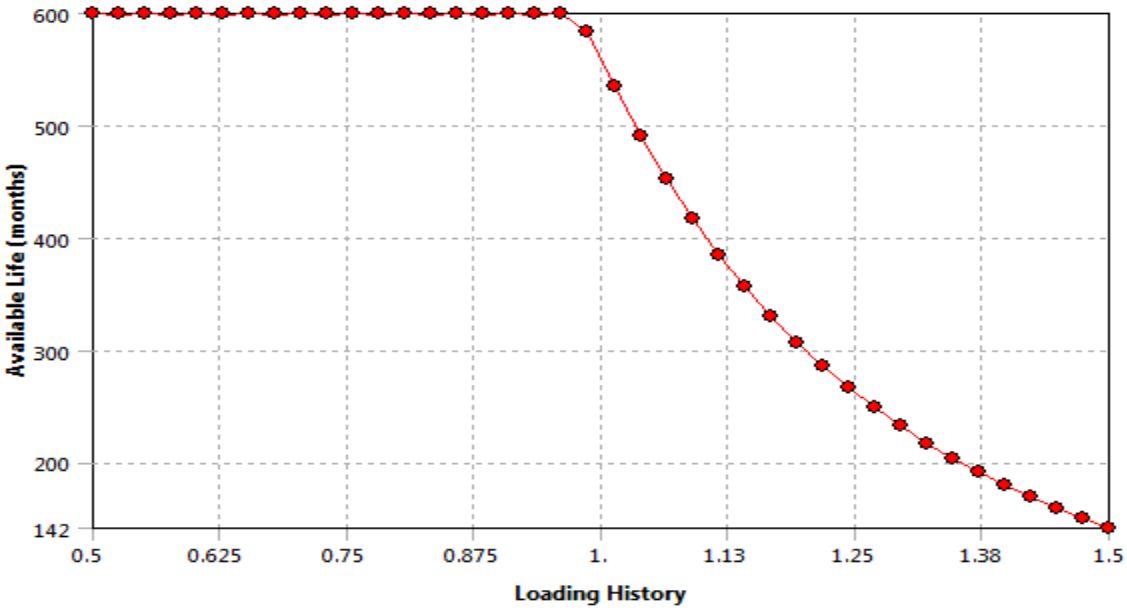

Figure 6.1 Strain life of tapered beam

2. Circular end cantilever beam

Strain life predictions of circular end beam are shown in Figure 6.2. A simulation result clearly reveals that design works well nearly up to a force limit of 129 N. After this limit of force design starts to lose its strain life. Minimum life of strain in the design is 382 months that is at 150 N.

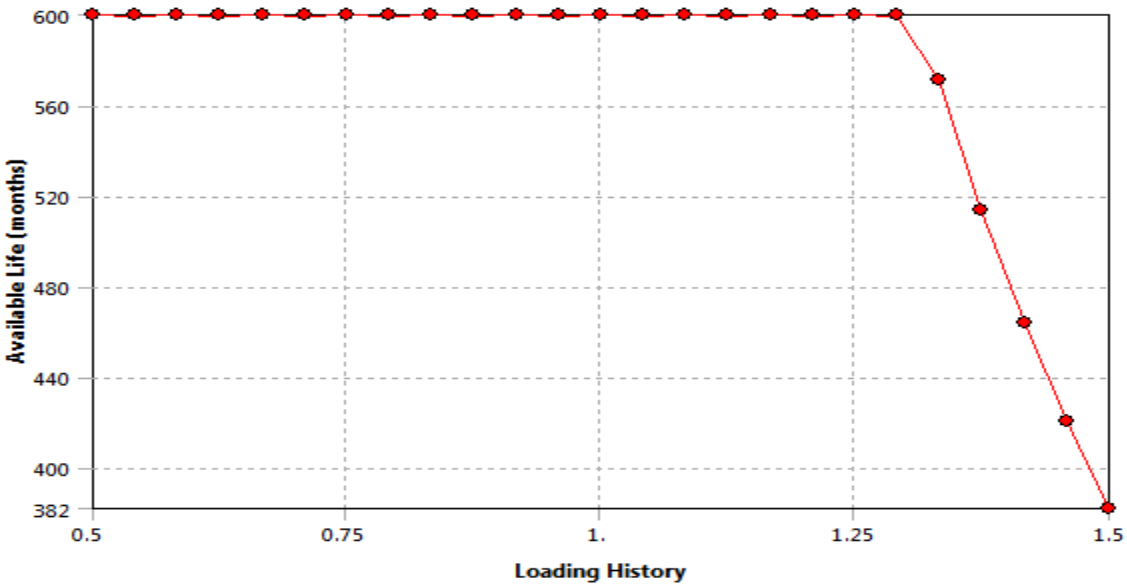

Figure 6.2 Strain life of circular end beam

3. Rectangular cantilever beam

Simulation results of strain life for rectangular cantilever beam are obtained as shown in Figure 6.3. Design does not lose its strain life up to a limit of 129 N. Minimum life of strain in the design is 365 months which occur on 150 N of force.

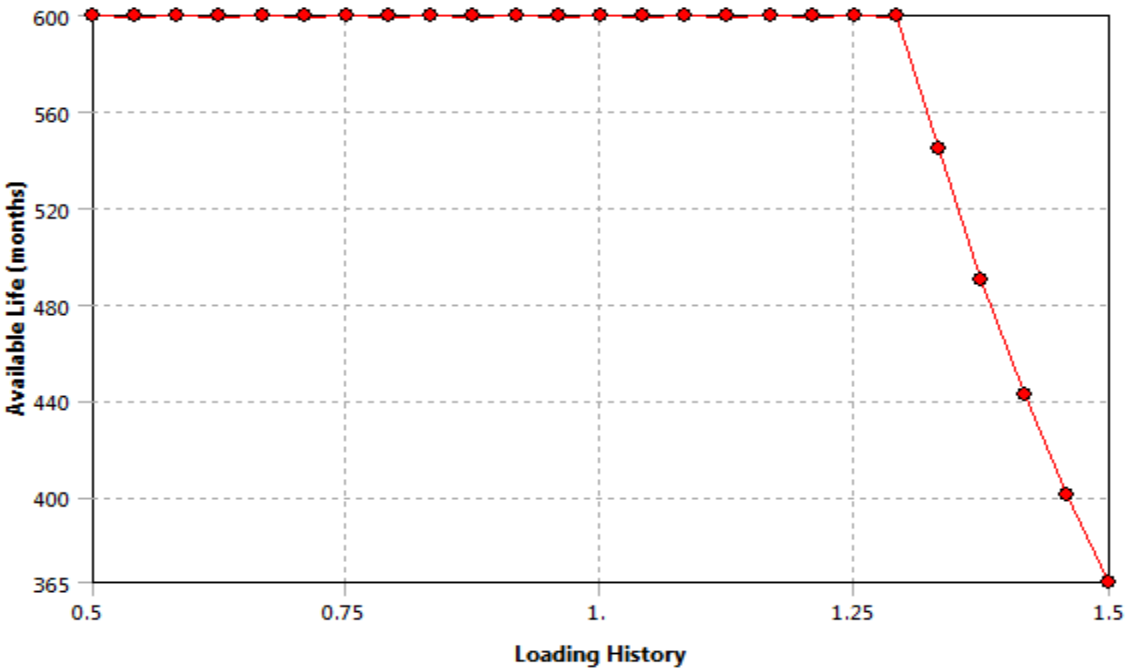

Figure 6.3 Strain life of rectangular beam

4. Squared frame beam

The simulation result in Figure 6.4 show the strain life behavior of squared frame beam with different percentage of force. Graph clearly indicates a stable life of strain of 600 months even beyond limits of 150 N.

5. T-shape cantilever

Figure 6.5 is a simulation result of strain life with different percentage of applied force of 100 N. It should be easily predictable from this information that the strain life of 600 months show constant behavior up to 66 N of force, after that the decrement in strain life starts and ends at 150 N with a minimum life of 45 months. At a desired force of 100 N the design has strain life of 170 months.

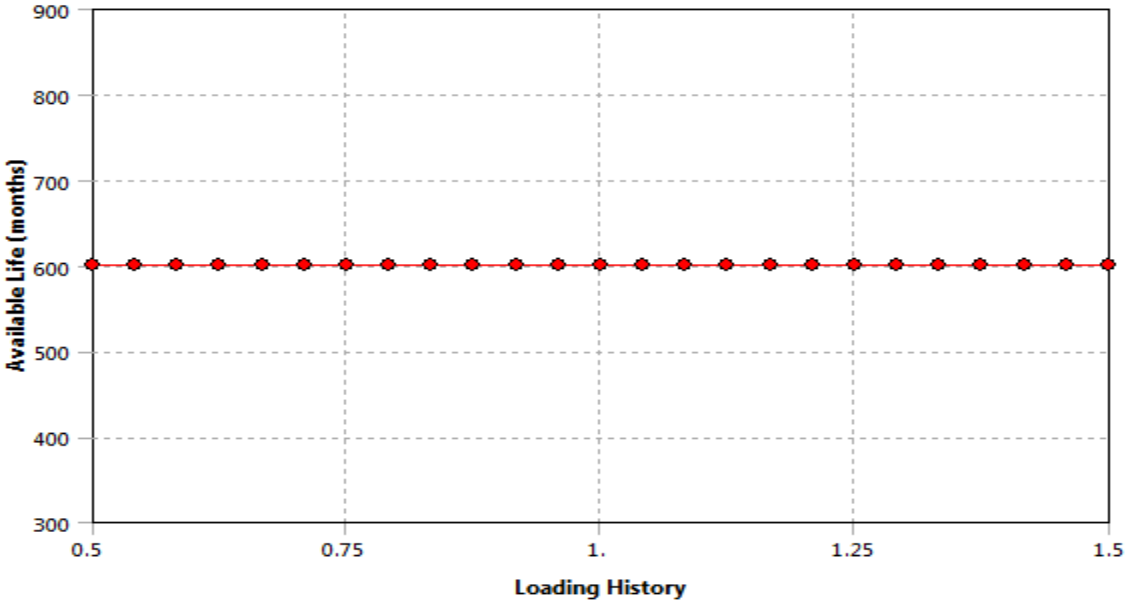

Figure 6.4 Strain life of squared frame

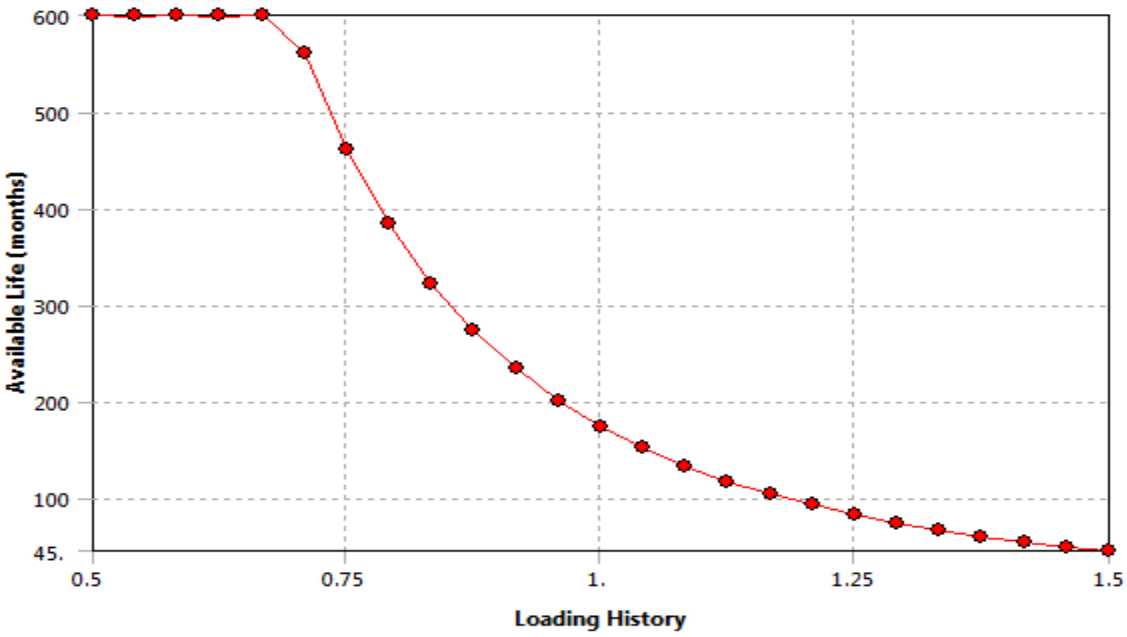

Figure 6.5 Strain life of t-shape beam

6.3.3 Stress life curves of different designs

Different materials have different life of stress it is significantly affected by shape of the design. Mean and alternating values of stress are included in engineering data of ANSYS workbench.

Then fatigue sensitivity curves have been obtained which contains life along y-axis and percentage of applied force (100 N) from 50-150 % along x-axis. Again it should be noted that these curves are plotted for the case when load of 100 N generates maximum deformation in the geometry of beams and that is possible only for a case when load is on end face of beam as shown in Figure 5.9.

1. Tapered cantilever beam

Design has maximum life of stress of 1440 months at 50 N force then it decreases rapidly with increasing amount of force. At 100 N of force, stress life of 135 months has been Obtained. Minimum life of stress is 49.5 months at a load of 150 N.

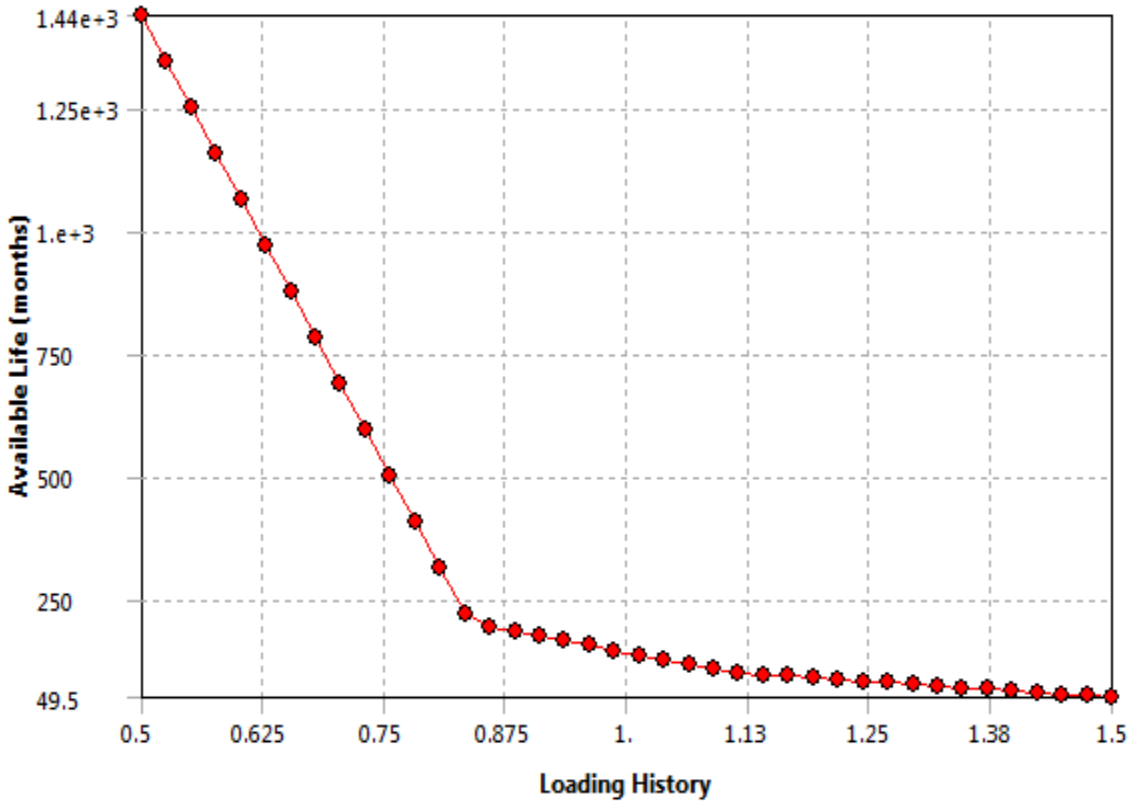

Figure 6.6 Stress life of tapered beam

2. Circular end cantilever beam

Maximum value of stress life corresponds to 1900 months at a load of 50 N. There is a rapid

Decrement in stress life as the value of load is increasing. At a force of 100 N the stress life of 531 months has been predicted. Minimum value of stress life corresponds to 98.8 months.

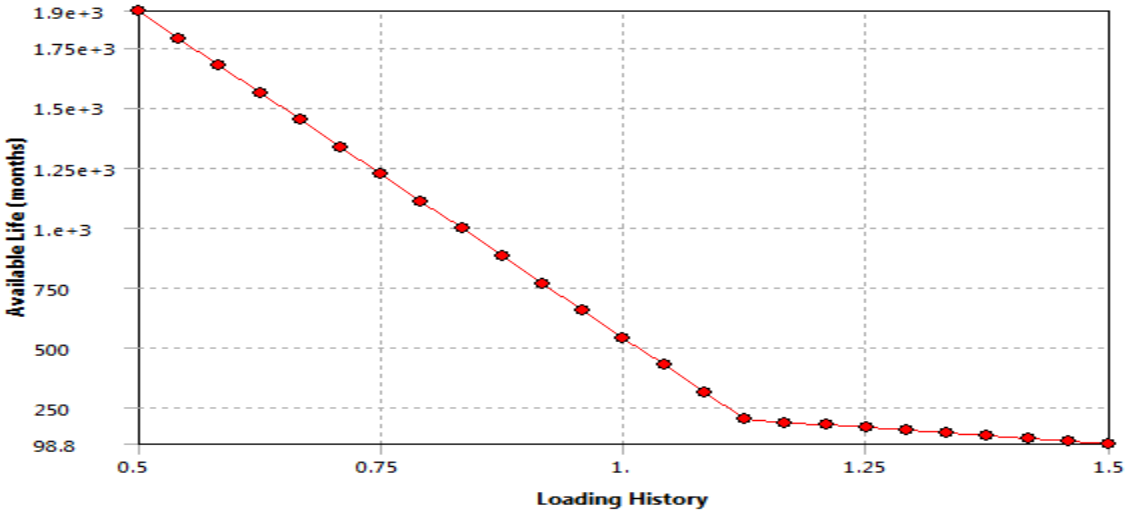

Figure 6.7 Stress life of circular end beam

3. Rectangular cantilever beam

Simulation result for stress life of rectangular cantilever beam is shown in Figure 6.8. Maximum stress life of 1880 has been obtained at a force of 50 N. Stress life of 500 months should be observed at a load of 100 N. Minimum life of this design is 96.7 months at a load of 150 N.

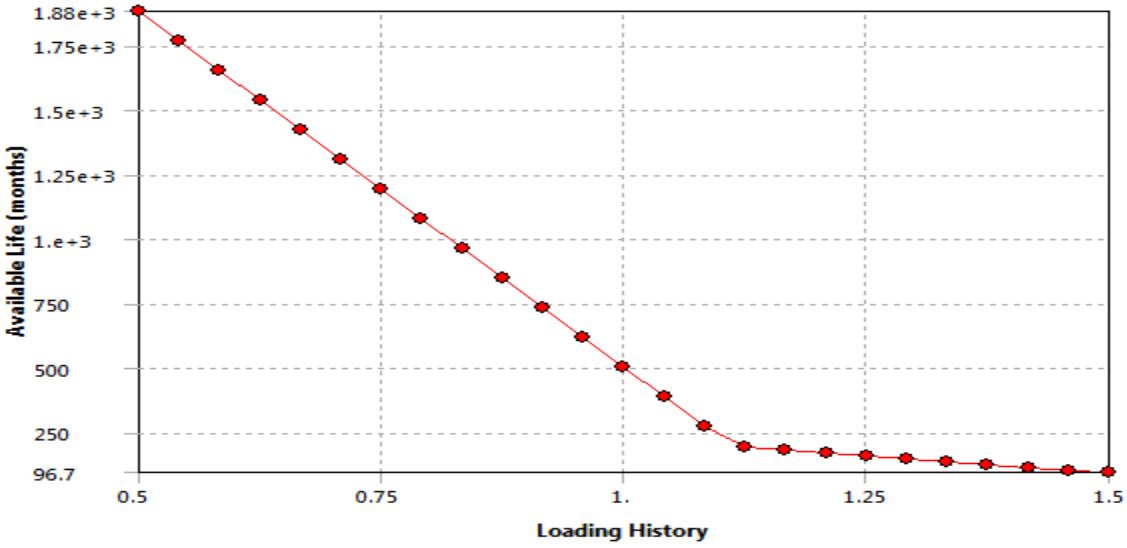

Figure 6.8 Stress life of rectangular cantilever beam

4. Squared frame beam

This structure corresponds to maximum stable values of stress life that are 1000000 months up to 75 N of force. At 100 N of force the stress life value is 250000 months. The minimum value occurred at 150 N is 67600 months.

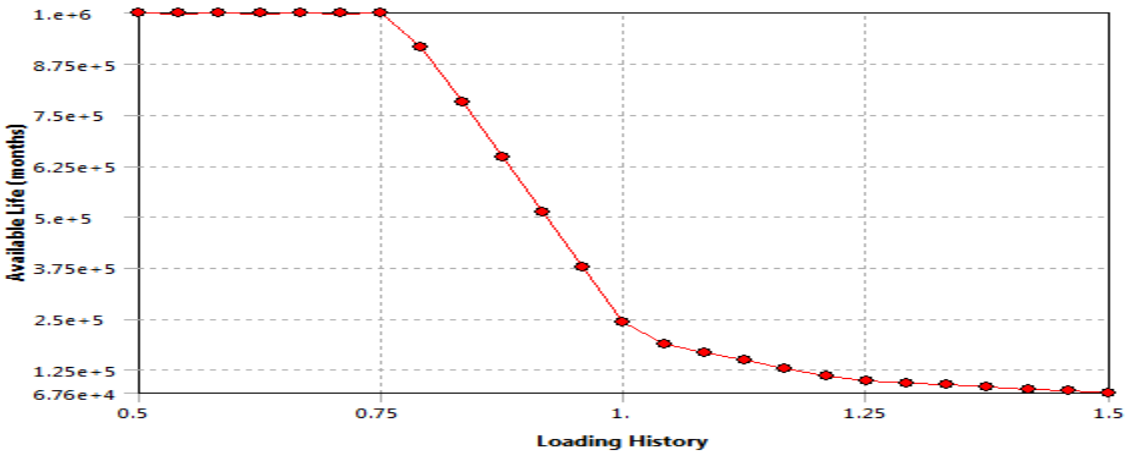

Figure 6.9 Stress life of squared frame

5. T-shape cantilever beam

Stress life of 687 months is observed at 50 N. At a force of 100 N stress life of 56 months has observed. It has minimum life of 24.2 months at a force of 150 N.

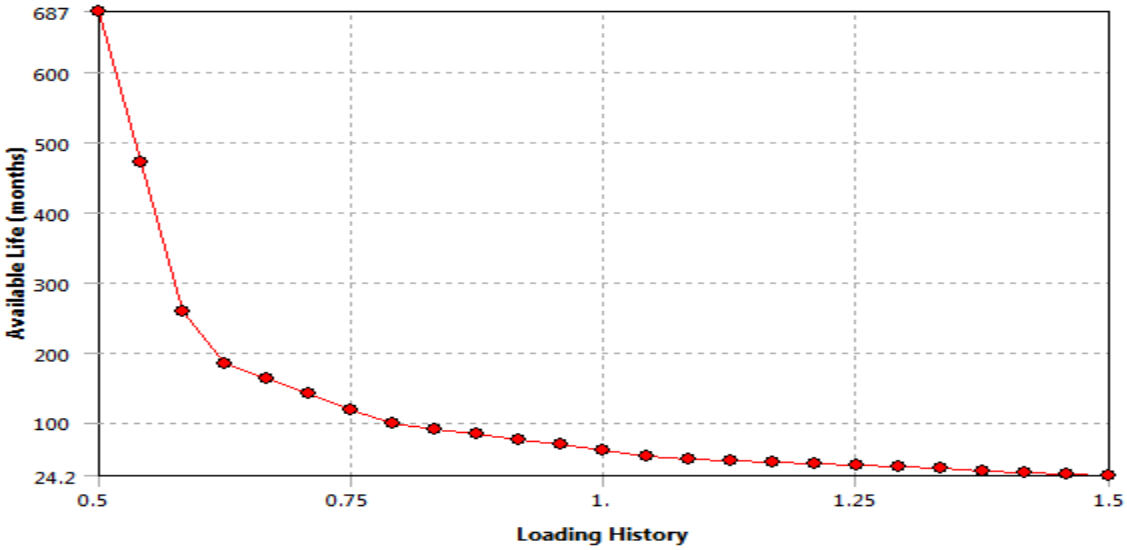

Figure 6.10 Stress life of t-shape beam

Chapter 7

Results and discussion

7.1 Comparison of sensitivity to load for different designs

For the purpose of analyzing sensitivity of different designs, force of 100 N is applied at a position where maximum disturbances or distortion occurs in a particular geometry. Change in strain, stress and deformation values have been obtained as shown in Figure 7.1. We will observe that T-shape structure is maximum sensitive design of cantilever beam, while squared frame geometry is least sensitive structure. Tapered beam structure is with good sensitivity to strain, stress and deformation, while circular end and rectangular cantilever beam are the structures of moderate sensitivity.

Table 7.1 Maximum values possible at 100 N

Type	Strain(mm/mm)	Stress(MPa)	Deformation(mm)
Squared frame	0.00020408823	39.3897283	2.09E-03
Rectangular	0.0017450043	336.78343	0.16908
Circular end	0.00185609103	358.221769	0.24945
Tapered	0.0023078563	445.42396	0.30075
T-shape	3.2608e-003	629.33	0.39939

Figure 7.1 shows the graph of change in strain values of different structures with changing force of 10-100 N. T-shape structure is found to be maximum sensitive, while squared frame is least sensitive one.

7.2 Effect of changing position of load

The different four structures rectangular, t-shape, circular end and tapered beams have been studied out. Application of load on front face is a practical case of analysis for the purpose of detecting slip in prosthetic hand. We have applied force in a circular area having diameter 3mm at a distance of 20 mm away from beam root assuming it to be a location of fingertip. If this centre of force is shifted to midway as shown in Figure 5.11 there is a significant decrement in the values of strain.

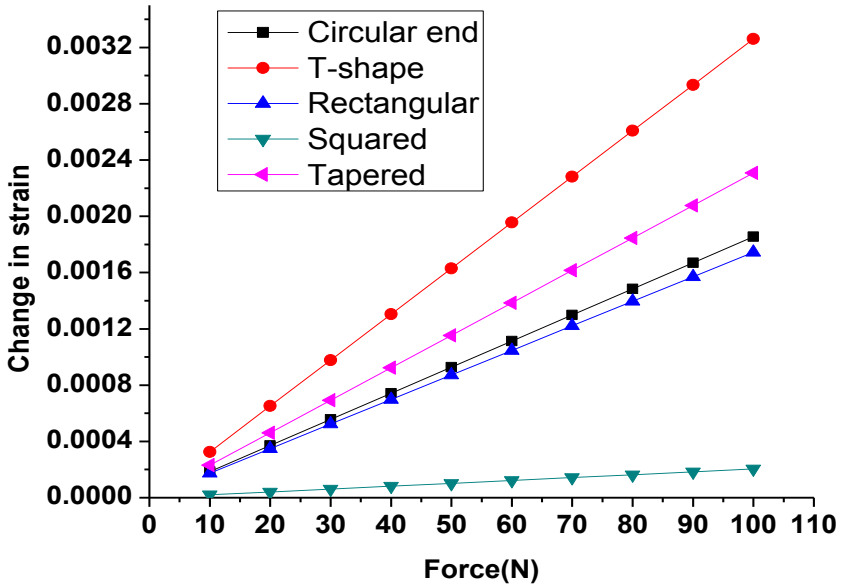

Figure 7.1 Change in strain v/s force

Table 7.2 shows the effect of changing position from 20 mm to 10 mm, percentage decrement in the values of strain, stress and deformation have been calculated.

Table 7.2 Percentage decrement in different values

Type of structure	Percentage of decrement		
	Change in strain	Change in stress	Deformation
Rectangular	57.43	57.28	80.23
Tapered	58.19	58.15	79.83
Circular end	63.39	63.44	81.68
T-shape	75.02	75.03	82.21

The percentage decrement value of 57.43 in strain for rectangular beam indicates that the force of 42.57 N at 20 mm produces same effect that is generated by the force of 100 N at 10 mm. Nearly 75 % decrement in the values of stress and strain comes for T-shape geometry, while 82.21% decrement is observed in deformation values. Minimum decrement is observed for a case of rectangular beam, which is also comparable to the values of tapered beam structure.

7.3 Comparative analysis of strain and stress life at different forces

Table 7.3 Strain and stress life at different forces

Type	Strain life (in months)			Stress life (in months)		
	50 N	100 N	150 N	50 N	100 N	150 N
Rectangular	600	600	365	1880	500	96.7
Tapered	600	570	142	1440	135	49.5
Circular end	600	600	382	1900	531	98.8
t-shape	600	170	45	687	56	24.2
Squared	600	600	600	1000000	250000	67600

Table 7.3 shows the life of strain and stress (in months) at different three forces of 50, 100 and 150 N. We have fixed 600 months as sufficient life of our design. It should be easily predictable from the data available in Table 7.3 that squared frame beam is the design of maximum strain and stress life, while t-shaped beam is a design with minimum life of strain and stress. Although we have analyzed both strain and stress life of all the different designs, but for our purpose of detecting slip in prosthetic hand only strain life analysis is sufficient. Because the sensing materials that have to be printed on these cantilever beams just use the strain effects in the structure of beam.

Although T-shaped beam is a maximum sensitive structure, but in this case our design life of 600 months is acceptable only up to a force limit of 66 N as shown in a Table 7.4, which represents the limit of forces up to which the design life of 600 months is reachable.

Table 7.4 Desired life and force limit

Type of structure	Force limit
t-shaped cantilever beam	66N
Tapered cantilever beam	95N
Circular end cantilever beam	129N
Rectangular cantilever beam	129N
Squared frame beam	>150N

7.4 Conclusion and future work

ANSYS simulation tool has been used for the structural analysis of different cantilever designs possible. Force of 10-100 N is applied and corresponding Change in stress, strain and deformation values are revealed at different load position. At end face loading position as shown in Figure 5.9, maximum disturbance of geometry occurs, that is a theoretical approach taken for various structural analyses, and is pretty useful for identifying location for piezostrain and piezostress sensors on different cantilever beams. But for our purpose practical application of load is on front face as shown in Figure 5.10, it is because the cantilever designs are made for a fingertip slip detection sensor in prosthetic hands. Results by shifting position of load from 20 mm to 10 mm are generated and significant decrement in the values of stress, strain and deformation have been observed. Also the effects of increasing contact area of force are being studied and reveal that it generates negligible effects on stress, strain and deformation values. Stress and strain life of different designs is obtained under fatigue analysis study.

T-shape beam is found to be a maximum sensitive design while squared frame beam is the least sensitive structure. The strain life of t-shape geometry is 170 months at a load of 100 N, as shown in Table 7.3, its strain life works well only up to a force limit of 66 N which is good for daily life activities. But the disadvantage related with T-shape design is its much sensitivity to change of load positions, Table 7.2 shows that there is decrement of 75 % in the values of stress and strain when load is shifted from 20 mm to 10 mm. On the other hand squared frame beam has strain life of 600 months even beyond the limit of 150 N shown in Table 6.4. But squared frame geometry has very low sensitivity that is not up to the mark. This geometry may be advantageous for heavy force measurements. Rectangular and circular end beams are of moderate sensitivity as predicted from Table 7.1 and shown in Figure 6.1. Both these structures have good strain life of 600 months up to a force of 129 N shown in Table7.4. These shapes are comparatively less sensitive to change of position of load. The percentage decrement in strain and stress values by shifting position from 20 mm to 10 mm is 57 % and 63 % for rectangular and circular end respectively as shown in Table 7.2. Tapered beam structure is the most compatible design among all these shapes. It has good sensitivity shown in Figure 7.1, moderate sensitivity to changing position of load that is nearly 58 % shown in Table 7.2 and design life of 600 months is attainable up to 95 N of force as predicted from Table 7.4, which is much suitable

for power grasps also. So depending upon the need of holding heavy or light loads, the particular design is selected which will be able to apply desired force. Normally the designs having force range from 65 to 100 N are being used in prosthetic hand applications. Tapered and T-shape beams are most efficient designs.

In the future works the suitable Locations for active and passive resistors along with piezoelectrics and thermistors can be identified. After that the fabrication of the device can be carried out. PZT (lead zirconate titnate) is the most use full material as piezoelectric which can be used for the purpose of detecting slip, while different piezoresistive materials can be used for the purpose of force measurement. A thermistor can also be inserted for the purpose of temperature detection.

References

1. Hardeep S Ryait, AS Arora and Ravinder Agarwal, 'Interpretations of wrist/grip operations from SEMG signals at different locations on arm', IEEE Transactions on Biomedical Circuits and System, vol.4, no.2, pp 101-111, 2010

2. Mark R Tremblay, Mark R Cutkosky, 'Estimating friction using incipient slip sensing during a manipulation task', IEEE International Conference, Robot Automation, Stanford, vol. 1, pp 429–434, 1993

3. A Mingrino, A Bucci, R Mangni, and P Dario, 'Slippage control in hand prosthesis by sensing grasping forces and sliding motion', IEEE Conference, Intell Robots System, Advanced Robotic System. Real World (RSJ/GI), Pisa, Italy, vol. 3, no. 3, pp 1803–1819, 1994

4. M Bergamasco, S Scattareggia, 'The mechanical design of Marcus prosthetic hand', IEEE International Workshop on Robot and Human Communication, Pisa, Italy, pp 95-100, 1995

5. R Magni, P Dario, R Lazzarini, 'An integrated miniature fingertip sensor', Seventh IEEE International Symposium on Micro Machine and Human Science, Seoul, Korea, pp 91-97, 1996

6. S Schulz, C Pylatiuk, G Bretthuer, 'A new ultra light anthropomorphic hand', Proceedings of IEEE International Conference on Robotics & Automation, Seoul, Korea, pp 2437-2441, 2001

7. MC Carrozza, B Massa, S Micera, R Lazzarini, M Zecca, P Dario, 'The development of a novel prosthetic hand- ongoing research and preliminary results', IEEE Transactions on Mechatronics, vol. 7, no. 2, pp 108-114, 2002

8. PH Chappel, Jamie A Elliott, 'Contact force sensor for artificial hand with digital interface for a controller', Measurement Science and Technology, pp 1275-1279, 2003

9. A Cranny, DPJ Cotton, PH Chapel, SP Baby and NM White, 'Thick film force, slip and temperature sensors for prosthetic hand', Measurement Science and Technology, vol. 16, pp 931–941, 2005

10. Lucia Beccai, Stefano Roccella, Alberto Arena, Francesco Valvo, Paolo Dario, 'Design and fabrication of a hybrid silicon three-axial force sensor for biomechanical application', Sensors and Actuators, pp 370–382, 2005

11. SP Beeby, PH Chapel, NM White, Darryl PJ Cotton, 'A novel thick film piezoelectric slip sensor for a prosthetic hand', IEEE Sensors Journal, vol. 7, no. 5, pp 752-761, 2007

12. Christian Cipriani, Marco Controzzi, Fabrizio Vecchi, M Chiara Carrozza, 'Embedded hardware architecture based on microcontroller for the action and perception of a transradial prosthesis', Proceedings of the 2nd Biennial IEEE/RAS-EMBS International Conference on Biomedical Robotics and Biomechatronics Scottsdale, USA, pp 848-853, 2008

13. Daisuke Gunji, Yoshitomo Mizoguchi, Seiichi Teshigawara, 'Grasping force control of multi-fingered robot hand based on slip detection using tactile sensor', IEEE International Conference on Robotics and Automation, NSK, Tokyo, pp 2605-2610, 2008

14. Dirk Goeger, Nico Ecker and Heinz Woern, 'Tactile sensor and algorithm to detect slip in robot grasping processes', Proceedings of IEEE International Conference on Robotics and Biomimetics, Karlsruhe, pp 1480-1485, 2008

15. Erik D Engeberg, Sanford G Meek, 'Adaptive object slip prevention for prosthetic hands through proportional-derivative shear force feedback', IEEE International Conference on Intelligent Robots and System, Akron, pp 1940-1945, 2008

16. Christian Antfolk, Christian Balkenius, Goran Lundborg, Birgitta Rosen, Fredrik Sebelius, 'Design and technical construction of tactile display for sensory feedback in a hand prosthesis system', http://www.biomedical-engineering-online.com/content/9/1/50, 2010

17. Seiichi Teshigawara, Kenjiro Tadakuma, Aiguo Ming, Masatoshi Ishikawa, 'High sensitivity initial slip sensor for dexterous grasp', IEEE International Conference on Robotics and Automation, Alaska, USA, pp 4867-4872, 2010

18. MH Hermen Shen, 'Analysis of beams containing piezoelectric sensors and actuators', Smart Material Structure, pp 439-447, 1994.

19. C Huang, YY Lin, TA Tang, 'Study on the tip-deflection of a piezoelectric bimorph cantilever in the static state', Journal of Micromechanics and Micro Engineering, pp 530-534, 2004

20. Mario Gonzalez, Gregory Van Barel, Ann Witvrouw , Bart Vandevelde, 'Analysis of beam deflections in poly Si-Ge cantilevers', IEEE international conference on Thermal, Mechanical and Multiphysics Simulation and Experiments in Micro-Electronics and Micro-Systems, Euro Sime, pp 1-6, 2006

21. BG Sheeparamatti, MS Hebbal, RB Sheeparamatti, VB Math, JS Kadadevaramath, 'Simulation of biosensor using FEM', Journal of Physics International MEMS conference, pp 241–246, 2006

22. J Dean, MRJ Gibbs, T Schrefl, 'Finite-Element Analysis on cantilever beams coated with magnetostrictive material', IEEE transactions on Magnetics, vol. 42, no. 2, pp 283-288, 2006

23. Van Anh Ho, Dzung Viet Dao, Susumu Sugiyama, Shinchi, Hirai, 'Force/moment sensing during sliding motion using a micro sensor embedded in a soft fingertip', IEEE 10th Intl. Conf. on Control, Automation, Robotics and Vision, Hanoi, pp-161-166, 2008

24. Thet T Mon, MSM Sani, Rosli A Baker, and NMZN Mohamed, 'Design Analysis of Silicon Cantilever for Label-less Sensing using Finite Element Method', IEEE international conference on Mechatronic and Embedded System and Applications, Kauntan, Malaysia, pp 89-93, 2008